Effects of Flow Control on the Aerodynamics of a Tandem Inlet Guide Vane

Thomas W. Vandeputte

Thesis submitted to the Faculty of the
Virginia Polytechnic Institute and State University
in partial fulfillment of the requirements for the degree of

Master of Science
in
Mechanical Engineering

Dr. Wing Fai Ng, Chair
Dr. Clint Dancey
Dr. Ricardo Burdisso

January 19, 2000
Blacksburg, Virginia

Keywords: Flow Control, Boundary Layer Suction, Trailing Edge Blowing, Aerodynamic Loss, Inlet Guide Vane

Effects of Flow Control on the Aerodynamics of a Tandem Inlet Guide Vane

Thomas W. Vandeputte

(ABSTRACT)

An aerodynamic investigation was performed to assess the effectiveness of combined boundary layer suction and trailing edge blowing at reducing the blade profile losses and the wake momentum deficit of a cascade of tandem IGV's operating at realistic flow conditions. Two trailing edge blowing designs were tested: metal-angle blowing, which oriented the blowing jets very near to the blade exit angle, and deviation-angle blowing, which oriented the blowing jets at a significant deviation angle from the blade exit angle. Both blowing designs used the same boundary layer suction arrangement. A linear cascade of five IGV's was tested with a flap deflection angle of 40° and an inlet Mach number of 0.3. The Reynolds number based on the overall IGV chord length for these experiments was greater than 500,000. The inlet and exit angles of the IGV at this flap setting were 0° and 55°, respectively. Tests performed with no flow control showed significant suction surface flow separation that generated large wakes with high losses and large momentum deficits. The application of boundary layer suction reduced the baseline pressure loss coefficient and wake momentum thickness by 22%. A suction mass flow of 0.4% of the passage flow was used to obtain these results. The addition of metal-angle blowing with the suction resulted in total reductions of 48% and 38% for the pressure loss coefficient and wake momentum thickness. A blowing mass flow of 3.1% of the passage flow was used in addition to 0.4% suction mass flow to obtain these results. The application of the deviation-angle blowing was detrimental to the aerodynamics of the IGV, as both the pressure loss coefficient and wake momentum thickness increased slightly over their suction-only values. This was attributed to a manufacturing defect which distorted the flow of the blowing jet. The results of the deviation-angle blowing experiments were not considered representative of the design intent and reinforced the importance of the hole design for creating a proper blowing jet. While low speed tests of this cascade showed results and trends very similar to those of previous research, the application of flow control proved to be less effective at higher speeds due to the generation of significantly larger wakes.

ACKNOWLEDGEMENTS

I would like to thank Dr. Wing Ng for providing me the opportunity to conduct this research and for his overall guidance of this project. His assistance and direction ensured a successful outcome and has been greatly appreciated. I would also like to thank Dr. Clint Dancey and Dr. Ricardo Burdisso for their insight and valuable time serving on my advisory committee.

Special thanks are also extended to fellow students Lenz Chu, Justin Douglas, and John Evans for assisting me with my experiments in the wind tunnel. I would also like to commend Dr. Shiming Li for his willingness to assist me in any way needed. His advice and long hours in the wind tunnel were invaluable for keeping the program on schedule. I would also like to thank Todd Bailie for providing me with the big, red, comfy office chair and also for keeping me from taking any of this too seriously.

Finally, I would like to thank Johnny, Jamie, and Bill from the ME Department machine shop for their excellent work and for their expert advice on machining issues.

TABLE OF CONTENTS

LIST OF FIGURES

LIST OF TABLES

NOMENCLATURE

B	Blowing ratio
C	Overall IGV chord length
C_s	Non-dimensional management mass flow
c_μ	Steady blowing momentum coefficient
$<c_\mu>$	Oscillatory momentum coefficient
C_Q	Suction coefficient
DP	Differential Pressure
IGV	Inlet Guide Vane
LFE	Laminar Flow Element
M	Local Mach number
M_∞	Free stream Mach number
P	Static Pressure
P_t	Total Pressure
Re	Reynolds number based on chord length
S	IGV span width
T	Static Temperature
T_t	Total Temperature
u	Local flow velocity
U_∞	Free stream flow velocity
VGJ	Vortex Generator Jet
α	Blade camber angle
γ	Specific heat ratio for air (= 1.4)
θ/d	Dimensionless momentum thickness
ρ	Density
ω	Area-averaged pressure loss coefficient

Subscripts:

1	Inlet conditions
2	Exit conditions

Chapter 1.0 INTRODUCTION

1.1 Background

Gas turbines are designed to operate ideally at one operating point and efficiently over a small operating range around that design point. Operation of a gas turbine at conditions far from the design point results in phenomena, such as flow separation, that lead to high losses and low efficiency. As the engine is operated further from the design point, losses continue to increase until the blading ultimately stalls.

One method for increasing the useful operating range of an engine is to use tandem blade rows in place of single blade rows. Tandem blading allows for variable blade cambers that can accommodate large variations in pressure ratio in rotor applications or large variations in volume flow and flow deflection in guide vanes and stators. The gap between the blade tandems is typically shaped to accelerate and guide the flow from the pressure surface of the front tandem onto the suction surface of the back tandem. The gap-nozzle energizes the wake from the front tandem and promotes sustained flow attachment on the suction surface of the back tandem (Saha and Roy, 1996). Generally, a tandem blade can achieve larger variations in operating conditions with greater efficiency than a single blade (Saha and Roy, 1996). Figure 1.1 shows the geometry of a typical tandem blade arrangement.

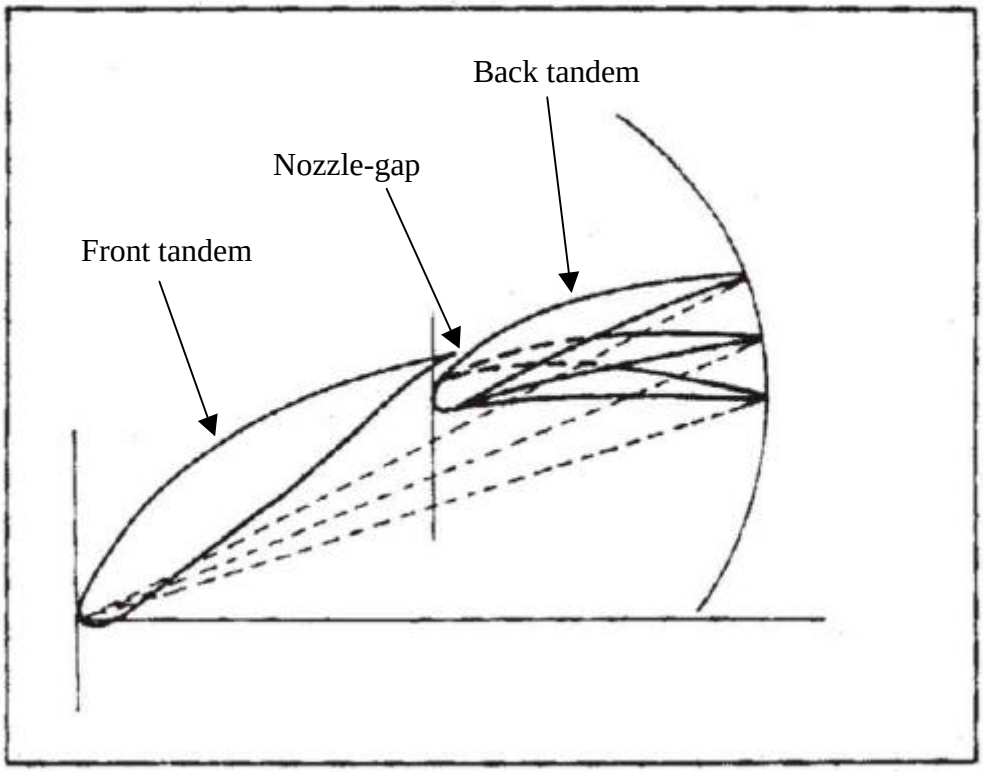

Figure 1.1 Tandem Blade Arrangement used by Saha and Roy (1996)

The blade studied in this experiment was a tandem inlet guide vane (IGV). It consisted of a back tandem with a circular leading edge located directly behind a front tandem with a blunt trailing edge. There was a negligible gap between the front and back tandems. This arrangement provided no flow guidance from the front tandem to the back tandem. As a result, the baseline flow for the IGV cascade showed significant suction surface flow separation. Large viscous regions, such as the separated flow region and the blade wake, introduce losses and unsteadiness into the flow. High losses lead to decreased engine efficiency, and unsteadiness causes vibration, noise generation, and decreased engine life (Lakshminarayana, 1996).

To reduce the effects of the flow separation and the blade wake, two flow control techniques were used. Boundary layer suction was applied to the suction surface of the back tandem, and trailing edge blowing was applied to the back tandem. The general goals of boundary layer suction and trailing edge blowing are to reduce the viscous and turbulent dissipation and mixing

associated with the loss generation. Boundary layer suction, shown schematically in Figure 1.2, attempts to reduce losses associated with the suction surface boundary layer and possible flow separation by removing a significant portion of the low-momentum fluid in these regions. Reducing the boundary layer thickness and separated region size results in reduced wake width and depth. Trailing edge blowing, shown schematically in Figure 1.3, attempts to reduce the mixing losses associated with the momentum deficit of the viscous wake region by introducing momentum directly into the wake. Reducing the momentum deficit results in a flatter velocity profile, which reduces shear stress and energy dissipation during the mixing process (Lakshminarayana, 1996).

Many studies have been conducted on the control of boundary layers and wakes for purposes ranging from understanding the physical phenomenon which dictate the success of various flow control techniques to evaluating the effects of flow control on engine acoustics. Experimental studies have been conducted on "simulated blades" involving axisymmetric wakes with no flow turning, airplane wings, and 2-D turbomachinery airfoil models. Most of the applicable experimental research has studied the effects flow control at low speeds (Park and Cimbala, 1991, Naumann, 1992, Waitz et. al., 1995, Sell, 1997, Bons et. al., 1999). Much of the research in the literature also focussed primarily on the noise reduction capabilities of flow control (Waitz et. al., 1995, Leitch, 1996, Sell, 1997). The following section highlights previous flow control research that, in conjunction with the capabilities of the current Virginia Tech test facility, influenced the design of the flow control system used in this experiment.

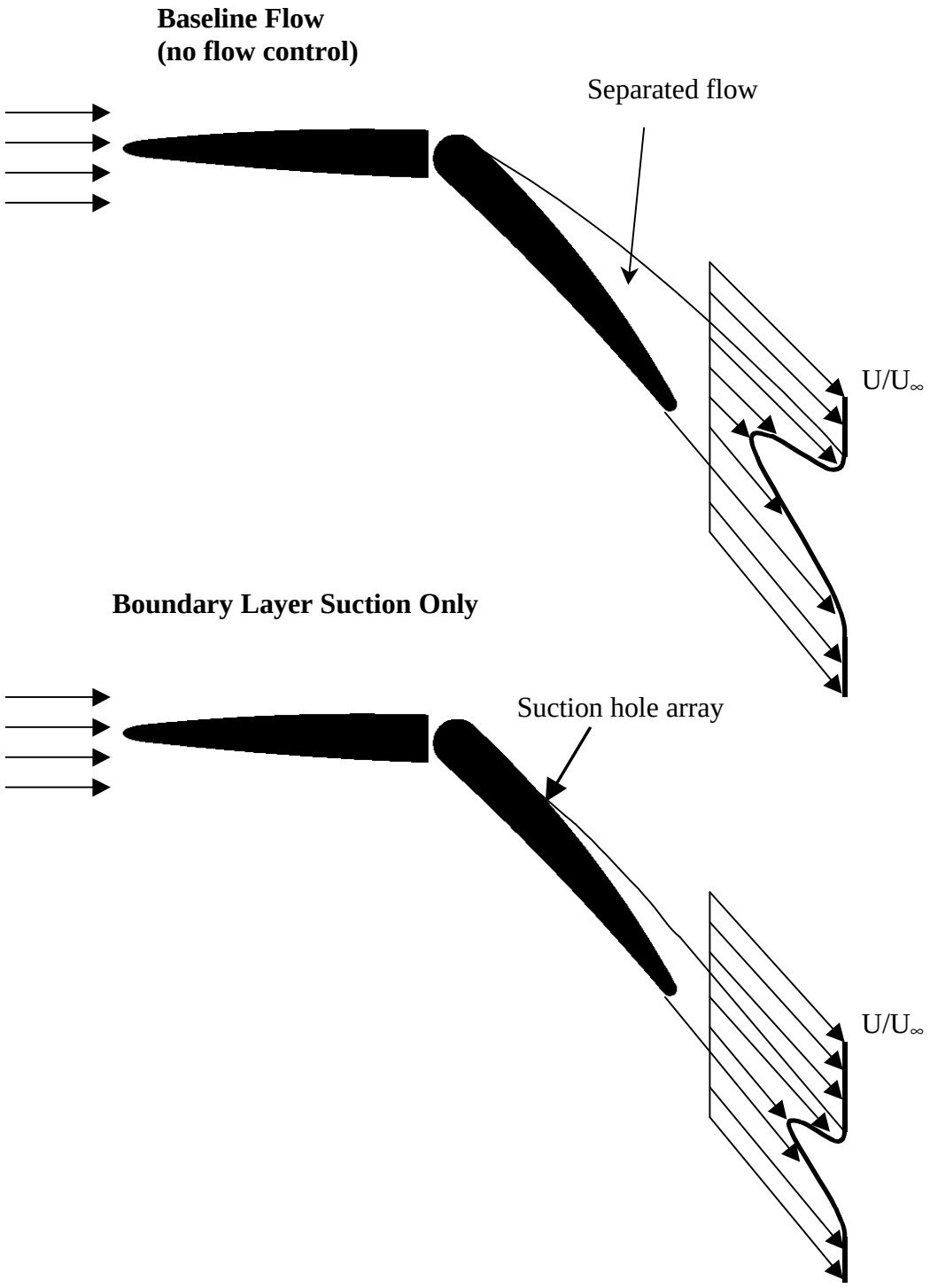

Figure 1.2 Schematic of Boundary Layer Suction Flow Control Strategy

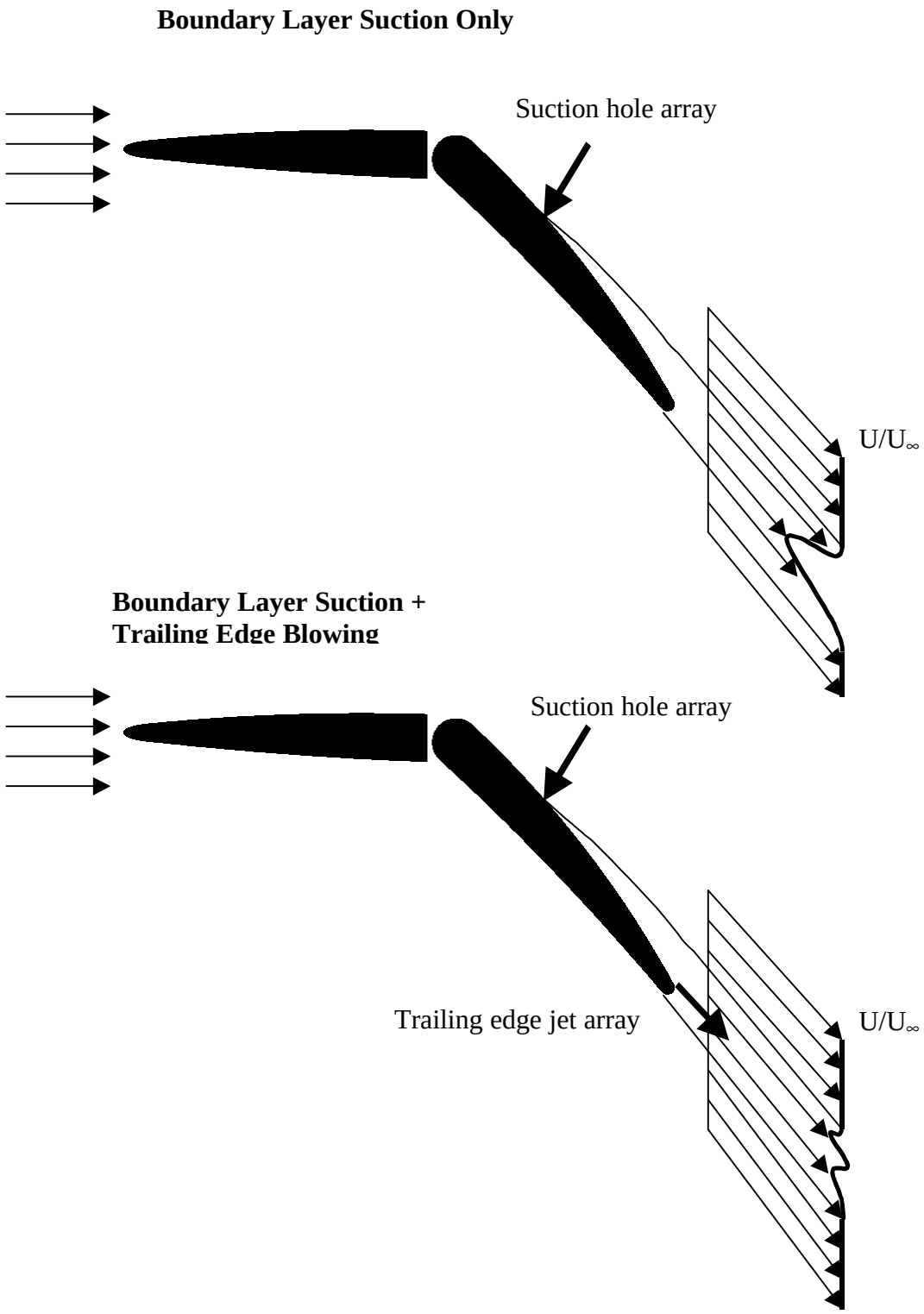

Figure 1.3 Schematic of Trailing Edge Blowing Flow Control Strategy

1.2 Previous Research

1.2.1 Simulated blade research

Some of the earlier flow control experiments involved examining momentumless wakes behind blade-like structures. These experiments focussed on understanding the physics of how trailing edge blowing affects wake attenuation and on determining blowing configurations that maximize these attenuating effects.

Park and Cimbala (1991) measured velocity profiles in the wake of a 2-D "airfoil" with and without trailing edge blowing. The airfoil consisted of a flat plate of constant thickness and induced no turning of the flow. Low speed wind tunnel tests (U_∞ = 4.2 m/s, Re ≅ 5400 based on plate length) were conducted for three blowing configurations: a central single slot, an asymmetric single slot, and a symmetric dual slot. The velocity profiles, for all blowing cases, showed local jet-like and wake-like regions that integrated to zero momentum deficit. The dual slot blowing configuration showed one velocity peak due to interactions between the individual jets. However, the center of this peak moved off of the centerline of the blade at some distance downstream of the trailing edge. The mean velocity profile of the dual jet wake was shown to flatten quickest (maximum velocity overshoot < 1% of U_∞ by x/d = 20), while the central single jet wake flattened slowest (maximum velocity overshoot < 1% of U_∞ by x/d = 45). However, the central single jet produced the slowest wake-width spreading rate while the dual jet produced the fastest growing rate. Therefore, at the same x/d position downstream of the trailing edge, the central single jet had the narrowest wake while the dual jet had the widest. Having shown that changing the initial conditions of the momentumless wake resulted in unique downstream effects, Park and Cimbala concluded that the flow field of a 2-D momentumless wake is strongly dependent upon the blowing configuration.

Research conducted by Naumann (1992) showed the dependence of wake attenuation on blowing geometry and initial conditions. Naumann measured mean and fluctuating velocity profiles behind a single blade model in a closed loop water tunnel. The blade consisted of a flat plate of constant thickness with no turning. Naumann compared results from a single continuous

blowing slot, a double continuous blowing slot, and a double discrete jet array. The tests were conducted such that fully turbulent flow conditions were attained. For all cases, the blowing slots or jets exited upstream from the trailing edge parallel to the trailing edge surface. For some experiments, Naumann also added vortex generators at the trailing edge of the blades. Naumann's results showed that the discrete jet arrangement was superior to the continuous slit blowing, as it resulted in quicker wake attenuation and smoother velocity profiles at the same axial location downstream of the trailing edge. The superiority of the discrete jet arrangement was attributed to enhanced mixing obtained by the discrete jets. The addition of the vortex generators improved the mixing even further, resulting in even quicker wake attenuation and smoother velocity profiles with lower blowing mass flow. A jet velocity of approximately four times the free stream velocity was required for the discrete jet blowing to effectively attenuate the wake.

1.2.2 Airplane wing research

Flow control experiments on flapped airplane wings have been conducted for quite some time with some of the older research dating back to the 1940's and 1950's. Although the flow fields of turbomachinery airfoils and airplane airfoils differ greatly, examining wing flow control provides an interesting analogy to the flapped design of the IGV's studied in this experiment. With airplane wings, the goals of flow control were to enhance the lift and reduce the drag of flapped wings. Poisson-Quinton and Lepage (1961) and Williams (1961) provide summaries of various 1940's and 1950's era flow control research, including several experiments involving boundary layer suction.

Poisson-Quinton and Lepage (1961) provided summaries of boundary layer suction experiments which had been conducted in France from 1946 to 1948. The experiments all applied boundary layer suction to deflected airfoil flaps. Tests were performed at Reynolds numbers similar to those experienced during landing conditions. These early experiments showed that the maximum gain in lift with the minimum suction mass flowrate was achieved by applying suction at the flap knee through a finely perforated surface. With a flap deflection angle of 45°, the flow

on the sucked flap was fully attached with a suction coefficient, C_Q, of 0.009. The suction coefficient was defined as shown in equation 1.1:

$$C_Q = q_v/U_0S \qquad (1.1)$$

In equation 1.1, q_v is the volumetric suction flow rate, U_0 is the free stream velocity, and S is the area of the wing corresponding to the spanwise extent of suction. Increasing C_Q beyond the fully attached limit resulted in no further increase in lift, indicating an upper limit for the effectiveness of suction.

Williams (1961) summarized similar experiments which had been conducted in England in 1954 with similar results. Flow separation over the flap seemed best prevented by starting suction about midway around the curved surface of the flap knee, the minimum pressure point. For large flap angles (about 60°), it was found additionally that the extent of the suction needed to be about 3% of the airfoil chord, and the ratio of the suction inflow velocity to the free stream velocity needed to be about 0.03. Similar to the French results, a constant increase in lift with increasing suction was achieved up until the point where flow was completely reattached.

Another method of flow control that had been successful for maintaining flow attachment on airfoil flaps is “knee blowing”. Knee blowing involved blowing air tangentially along the flap’s suction surface from near the leading edge of the airfoil flap. English experiments from 1954, as summarized by Williams (1961), showed that knee blowing could prevent separation at flap angles up to 75°. More recent experiments by Wygnanski (1997) compared steady knee blowing to oscillatory knee blowing. According to Wygnanski, oscillatory blowing “exploits the natural amplification of periodic disturbances by the boundary layer resulting in an effective transport of momentum across the flow”. Tests performed on an Eppler 214 airfoil of 11% thickness with a 30% flap deflected 20° showed a baseline lift coefficient, C_L, of 1.17. With the application of oscillatory blowing at a blowing momentum coefficient, $<c_\mu>$, of 0.3%, C_L was increased by 0.44. To achieve the same C_L increase with steady blowing, c_μ = 3% was required. The order of magnitude difference in the input momentum requirement was due to the increased mixing of the large eddies created by the oscillatory blowing. The steady blowing relied more heavily on the

jet momentum itself to control the flow. Further tests also showed that separation control by periodic forcing remained effective at higher free stream Mach numbers while steady blowing became less effective.

1.2.3 Turbomachinery airfoil research

Using much of the simulated blade research as discussed earlier in this chapter as a baseline, numerical and experimental studies have been performed to evaluate and optimize flow control techniques in setups which more closely model a turbomachinery environment. The goals of flow control applied to turbomachinery have largely been to reduce engine noise.

Kerrebrock et al. (1998) performed numerical design studies of a family of fan stages of varying tip speeds that use boundary layer suction. Starting from the von Karman integral momentum equation, Kerrebrock et. al. showed that for nearly separated flow, the reduction in momentum thickness is exponentially related to the distance downstream from the point of suction application. This indicated that a large amount of control over the downstream boundary layer thickness could be obtained with a small amount of mass flow removal. Kerrebrock et. al.'s numerical results, obtained using MTFLOW, and axisymmetric solver, MISES, a viscous, multiple blade cascade code, and FELISA, a fully 3-D transonic Euler solver, showed that the best location for suction was at the start of a strong pressure recovery region. Suction in this region resulted in the best overall fan stage performance with the least amount of suction mass flow.

Waitz et al. (1995) performed numerical and experimental studies of a high-bypass ratio fan blade design. The numerical results were obtained using MISES and UNSFLO, a 2-D thin shear layer, Navier-Stokes cascade solver. The numerical model of the fan blade applied boundary layer suction at 50%, 80%, and 90% chord on the suction surface at mass removal rates corresponding to 0%, 25%, 50%, and 75% local momentum thickness removal. The case which proved most effective applied suction at 90% chord with 75% momentum thickness mass flow removal (about 2% of the fan passage flow). For this case, the time-mean wake width was reduced by 21%, and the peak time-mean wake deficit was reduced by 40%. The presence of the

pressure side boundary layer and the finite thickness of the trailing edge limited the reductions in wake width and deficit that could be achieved by suction. Experimental cascade results on the same blade shape with suction applied at 80% chord with 70% local momentum thickness mass flow removal achieved reductions in the wake width and peak wake depth of 15% and 40%, respectively. Waitz et. al. used the experimentally obtained wake profiles to numerically estimate reductions in the amplitude of propagating circumferential acoustic modes. Mode amplitudes were reduced approximately 4 dB using boundary layer suction.

Sell (1997) performed a more comprehensive experimental study based on the work of Waitz et al. (1995). Sell performed low-speed cascade tests that compared boundary layer suction and trailing edge blowing in a more realistic flow field. Sell's cascade consisted of three first-stage Pratt and Whitney Advanced Ducted Propulsor blades (two complete passages) at a realistic angle of attack and takeoff flow conditions. Wake profiles were obtained at 0.5, 1.0, 1.5, and 2.5 chords downstream from the cascade exit. The boundary layer suction consisted of arrays of rectangular slots located at 50% and 80% chord on both the suction and pressure surfaces of the blade. Individual slot arrays were covered to test different suction configurations. Three separate trailing edge blowing configurations were tested: a single row of holes located at 91.2% chord at a 10° deviation angle, a single row of holes through the trailing edge at the blade exit angle, and a single row of holes where each hole alternated between the blade angle and the deviation angle. The configuration tested by Sell did not allow for simultaneous suction and blowing, and the baseline flow did not indicate the presence of suction surface flow separation.

For Sell's experiment (1997)The most effective suction configuration applied suction at 80% chord on the suction surface. With suction at this location, the momentum thickness was reduced by 50% with a 1.25% passage flow suction rate and by 58% with a 2.23% passage flow suction rate. 1.25% suction corresponded to a non-dimensional management mass flow, C_s, of 1.02, and 2.23% suction corresponded to a C_s of 1.83. C_s was defined as the management mass flow divided by the mass flow of the suction surface boundary layer displacement thickness. Sell's results showed that after complete removal of the boundary layer, which corresponds to $C_s = 1$, further suction provided little benefit. Similar to Waitz et. al., Sell also noted that boundary

layer suction for the reduction of momentum thickness was limited by the thickness of the trailing edge.

Sell achieved momentumless wakes for each of the three trailing edge blowing geometries tested. Momentumless wakes were achieved for the deviation, blade, and alternating blowing geometries with blowing mass flows of 1.08%, 1.02%, and 1.23% passage flow, respectively. All cases displayed local wake-like and jet-like profiles with some asymmetry, but the deviation-angle blowing achieved the most symmetric wake profile. The deviation-angle blowing also yielded the greatest reduction in turbulence intensity and wake depth relative to the baseline flow. Sell used the experimentally measured wake profiles to estimate the reductions in noise achieved by the three blowing geometries. The deviation-angle blowing produced the greatest estimated noise reductions: 24.4 dB, 18.6 dB, 13.2 dB, and 7.6 dB for the second through fifth harmonics of the blade passing frequency and 7.0 dB in broadband noise.

Rather than use suction, Bons et al. (1999) applied a blowing technique for separation control. Bons et. al. used vortex generator jets (VGJ) to reduce suction surface separation on a low-pressure turbine blade. The VGJ array consisted of jets oriented at a 30° pitch angle (angle from hole centerline to blade surface) and a 90° skew angle (orientation of the jet relative to the free-stream direction). This jet arrangement created a horseshoe vortex pair with one very strong leg and one weak leg of opposite sign. This design attempted to energize the separated boundary layer by transporting high momentum free stream fluid to the blade surface with the strong vortex leg. This method was verified both numerically and experimentally.

Bons et. al. tested a cascade of eight Pratt and Whitney PakB research blades, which are a scaled version of a typical highly-loaded low-pressure turbine blade. The tests were conducted at low speeds (Re = 50,000). Significant suction surface separation was measured and documented for the baseline flow. One of the middle blades of the cascade contained the VGJ array described above. The array was located at 73% chord, which was within the separated region of the blade. The VGJ flow control technique reduced the momentum thickness by 65% with a blowing ratio, B, of 0.6 to 1.0. The blowing ratio was defined as $(\rho u)_{jet}/(\rho u)_{local}$. Much like boundary layer suction, minimal gains were achieved when the blowing ratio was increased beyond the value

where flow reattached. Bons et. al. also noted that VGJ blowing produced no significant adverse effects when applied at higher Reynolds numbers where no initial flow separation was observed.

1.3 Objectives of the Current Experiment

Previous numerical and experimental work has shown that various mass addition and mass removal techniques have been successful at reducing velocity deficits and wake momentum deficits, which in turn were translated into reductions in engine noise. Much of the experimental turbomachinery research, however, was conducted at low-speeds. Additionally, there is little data that documents the effects of flow control on blade profile losses. To the authors knowledge, there has also been no prior research on flow control applied to a tandem blade arrangement.

The goals of this research were to apply flow control to a tandem inlet guide vane operating at a realistic Mach number and document the effects of the flow control on the pressure loss coefficient and on the wake momentum thickness. The inlet Mach number for the IGV cascade, which was nearly three times the Mach numbers used in previous experiments, was consistent with the landing approach conditions defined by the project sponsor for this blade. The resulting exit Mach number for the IGV cascade was more than five times greater than those achieved in previous cascade flow control experiments.

The flow control design consisted of boundary layer suction applied in conjunction with trailing edge blowing. The boundary layer suction was intended to reduce the suction surface flow separation, while the trailing edge blowing was intended to reduce the mixing effects of the blade wake. Two trailing edge blowing designs, metal-angle blowing and deviation-angle blowing, were implemented with one common boundary layer suction design.

The flow control's effects on the IGV aerodynamics were quantified through wind tunnel testing of a linear cascade of five IGV's. Due to facility limitations, flow control was applied to only the middle IGV of the cascade. Aerodynamic data that facilitated the calculation of the pressure loss coefficient and the wake momentum thickness was acquired during the tests. The loss

coefficients and wake momentum thicknesses obtained for runs implementing flow control were compared to the baseline values to quantify the effectiveness of the flow control. The results were also compared and contrasted to the low-speed results achieved in previous research. The suction and blowing mass flows used during the experiments were also measured to quantify the impact of the flow control on the blade passage flow. Tunnel flow control devices such as endwall suction and tailboards were not implemented during these tests.

Chapter 2.0 EXPERIMENTAL METHOD

The following chapter describes the experimental setup. Sections 2.1 and 2.2 describe the IGV cascade and the design of the flow control blade. Section 2.3 describes the wind tunnel facility. Sections 2.4 and 2.5 describe the flow control and instrumentation setup. Section 2.6 describes the flow visualization techniques, and section 2.7 describes the measurement and data reduction techniques.

2.1 Description of the cascade

The blades studies in this experiment were tandem IGV's designed for use in a gas turbine engine. Each IGV consisted of a front tandem and a back tandem blade section. The front tandem was fixed with a constant inlet blade angle, α_1, of 0°. The back tandem (flap) could pivot about its leading edge and thus had an adjustable exit angle, α_2. The distance between the leading edge and the trailing edge of the IGV changes depending on the flap position. The overall blade chord was defined as the sum of the front tandem's chord length and the back tandem's chord length in order for the overall chord to remain independent of the flap position. Different flap positions correspond to different flight conditions. The condition of most interest for flow control application was the "approach" condition. Table 2.1 summarizes the major geometric properties of the IGV cascade when operating at approach conditions, and Figure 2.1 shows a schematic of the IGV geometry at approach conditions.

Table 2.1

Blade Specifications, Approach Condition

Overall Blade Chord, C	3.2 inches
Pitch	1.912 inches
Span, S	6 inches
Inlet Blade Angle, α_1	0°
Flap Angle	40°
Exit Blade Angle, α_2	55.0°

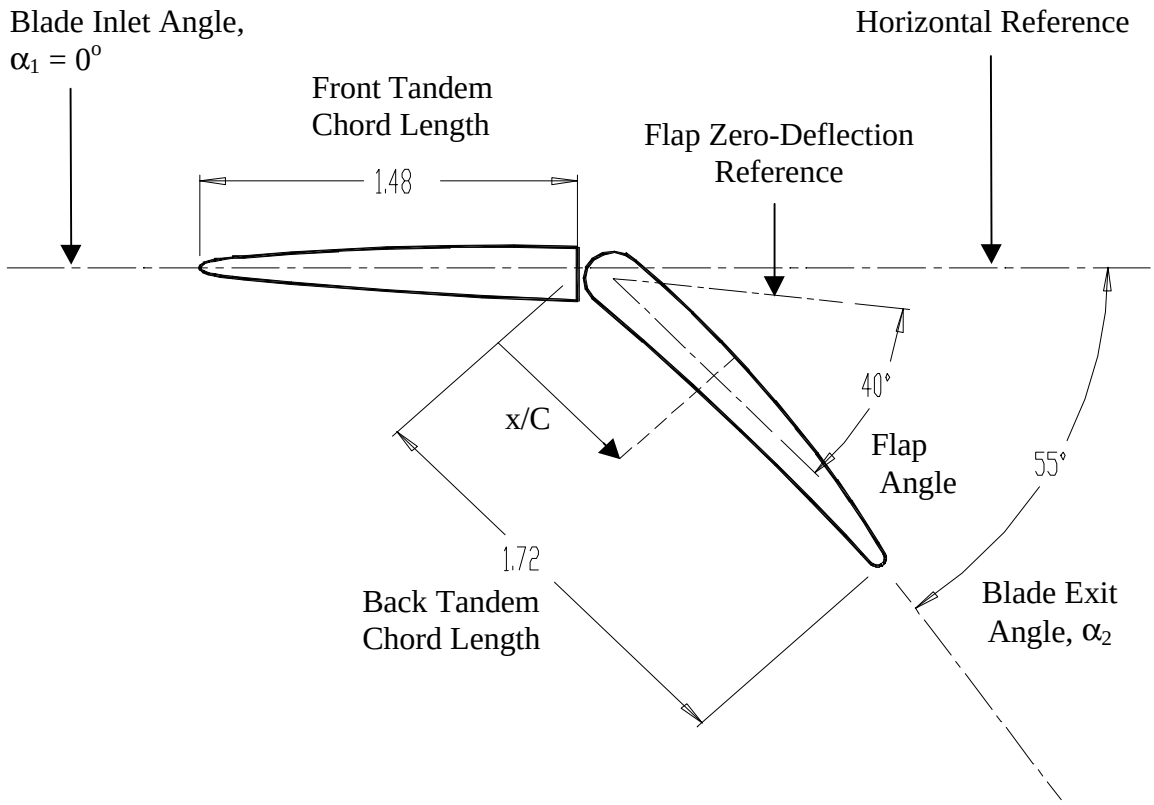

Figure 2.1 IGV Blade Geometry

The cascade consisted of Plexiglass sidewalls containing five complete IGV's. This formed four complete flow passages. Both the front and back tandem of each IGV was located and supported by two solid pins on each side. The back tandem of the flow control IGV, however, was supported by four hollow tubes and one solid pin on each side. Figure 2.2 shows the fully assembled cascade installed in the wind tunnel test section. The IGV's were numbered one through five, starting from the top. Blade three was the flow control blade.

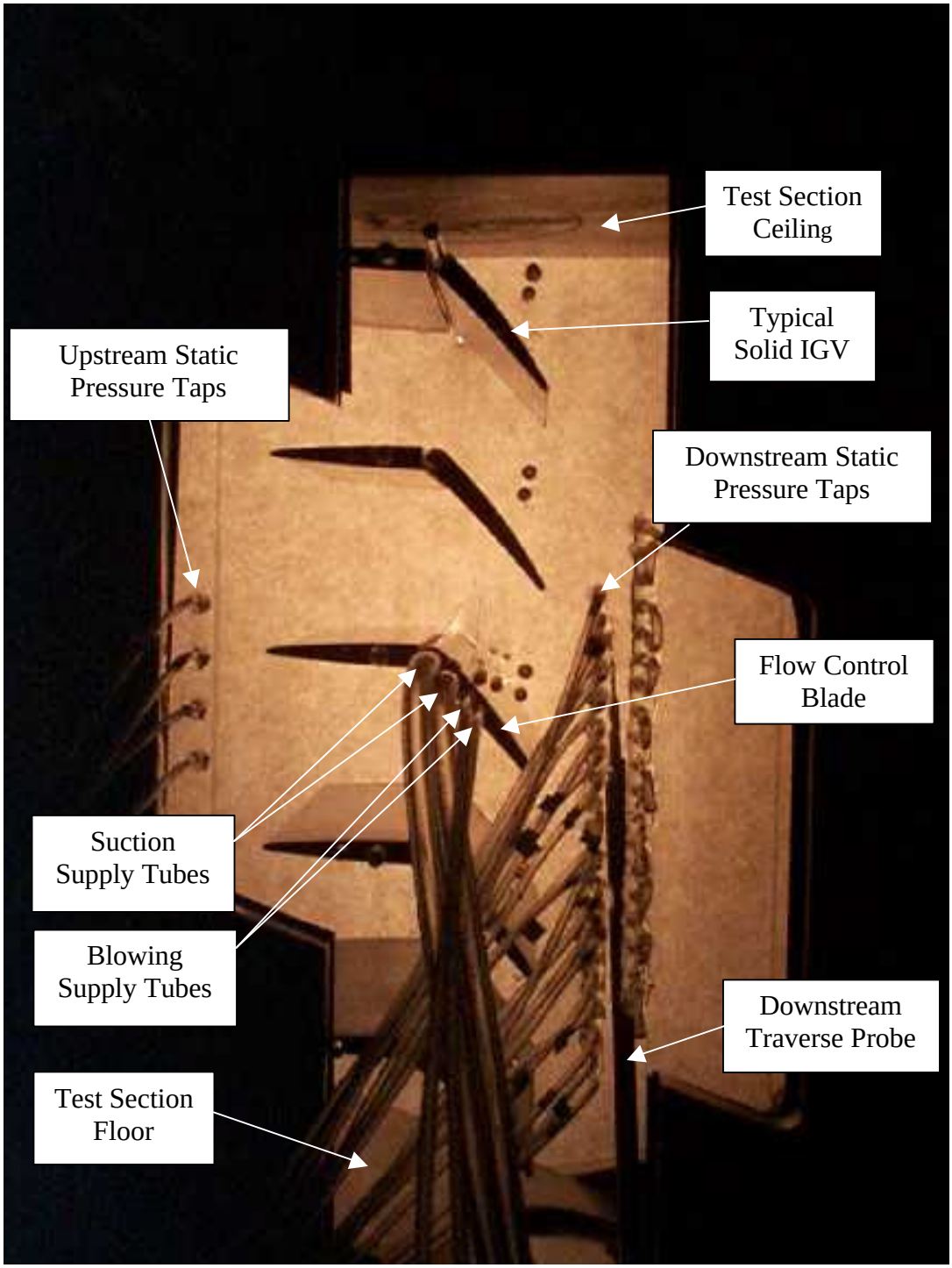

Figure 2.2 Assembled IGV Cascade Installed in Wind Tunnel

2.2 Description of the Flow Control Blade Design

The purpose of the flow control blade was to reduce aerodynamic losses through the blade passage. Schlieren photography and surface oil flow visualization of the baseline solid IGV were used in order to qualitatively understand the baseline flow. These flow visualization techniques, the results of which appear in Chapter 3, showed significant suction surface flow separation that originated near the leading edge of the back tandem. The separation did not appear to reattach, and thus a large wake with high losses was generated. The goal of the flow control design was to use boundary layer suction to reduce the suction side separation, thus reducing the wake width, and to use trailing edge blowing to reduce the wake depth.

2.2.1 Plenum and Connection Design

In order to provide a mass flow source for the boundary layer suction and trailing edge blowing, plenums within the blades were required. To accomplish the suction and blowing on the same blade, a dual plenum blade was designed. In order to maintain flexibility with the suction and blowing mass flows, the plenums were designed with nearly equal volumes. The thickness of the blade and the strength of the blade material limited the volumes of the plenums. Finite Element Analysis results from the sponsor mandated that the wall thickness of the blade be at least 0.050 inches. The partition between the suction and blowing plenums was also designed with this minimal thickness. The cross section of each plenum was constant through the entire blade. The flow control tandem was fabricated by EDM machining one of the solid, baseline back tandems.

Once the plenum design was complete, the plenum supply lines and blade end caps were designed. Two stainless steel tubes per side supplied each plenum. The suction plenum had two 0.118-inch and two 0.106-inch inner diameter supply tubes, and the blowing plenum had two 0.085-inch and two 0.071-inch inner diameter supply tubes. The supply tubes were attached and sealed to the blade with end caps machined to exactly match the cross sectional shape of the plenum. The end caps were machined with the same EDM programs used to make the plenums. They were recessed slightly into the plenums and permanently joined to the blade with silver

solder. The ends of the blade were ground smooth, and the holes for the supply tubes were drilled. The supply tubes were press-fit into the ends of the plenum and bonded with Loctite. Figure 2.3 shows an end view of the assembled flow control blade. The blade assembly was submersed in a tank of water, and 50 psig air was supplied to each plenum to verify that all joints were leak free.

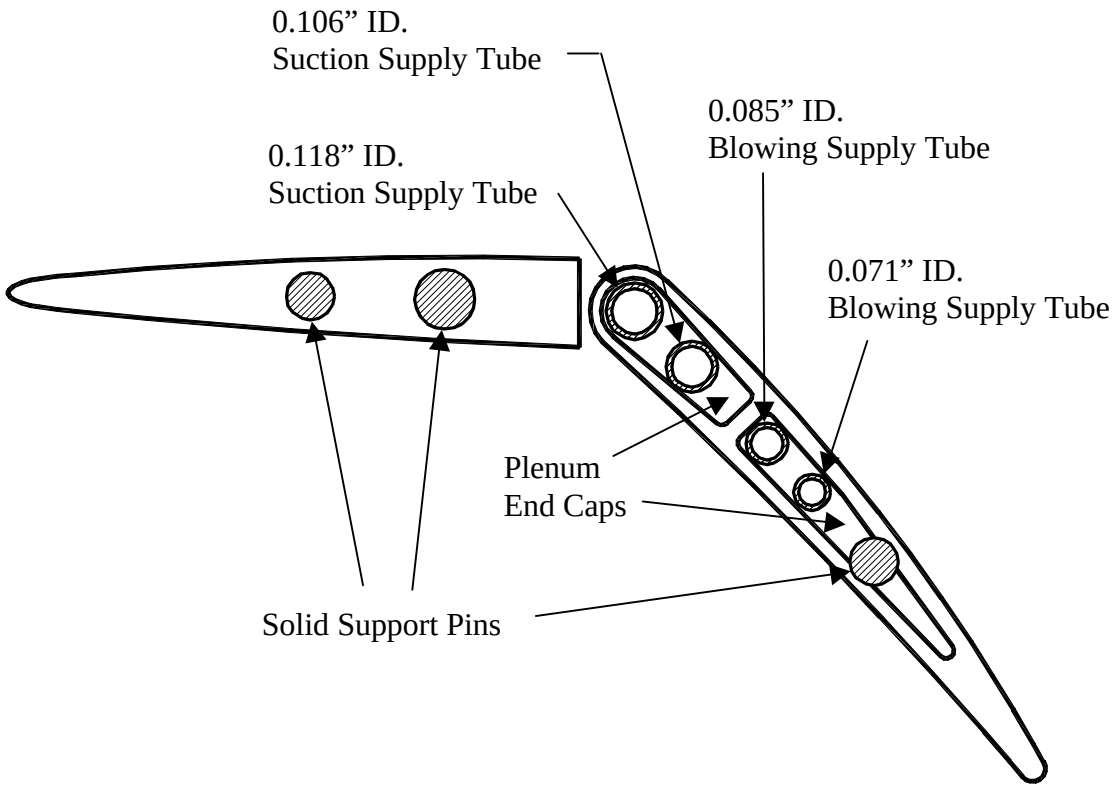

Figure 2.3 End View of Assembled Flow Control Blade

2.2.2 Boundary Layer Suction Design

The primary design parameters for the boundary layer suction geometry included:

- Number of suction hole arrays
- Number of suction holes per array
- Chord-wise location of the suction hole arrays
- Individual hole diameters
- Suction hole angle

The numerical and experimental results achieved by Sell (1997) and Waitz et al. (1995), as described in Chapter 1, showed that in the absence of separated flow, the best location for boundary layer suction is as near to the trailing edge as is physically possible. However, in cases with separated or nearly separated flow, Kerrebrock et al. (1998) and Poisson-Quinton and Lepage (1961) showed that the most effective location for suction is at the start of a strong pressure recovery region, where the flow separation is likely to begin. The location of the suction array was determined based on the qualitative data available from the Schlieren and Surface oil flow visualization photographs.

The final boundary layer suction design placed one array of 26 suction holes located at x/C = 0.59 on the blade suction surface. This location was near the point where separation became clearly visible in the Schlieren photographs. The hole array consisted of 1/32-inch diameter holes equally spaced 0.08 inches from center to center. The suction holes were angled towards the incoming flow at 70° from the local blade surface. The suction hole array was centered on the blade span, creating a two-inch flow control span over the back tandem with two-inch spans of non-controlled flow on both ends of the tandem.

The minimum suction mass flow required for flow reattachment was roughly estimated from the airfoil results presented by Poisson-Quinton and Lepage (1961). The minimum suction mass flow was calculated assuming a suction coefficient of 0.009 for the two inch flow control span and for the inlet conditions tested in this experiment. The maximum attainable suction mass

flow for this blade design was estimated by choked-flow calculations to be slightly greater than the minimum requirement estimation.

2.2.3 Trailing Edge Blowing Design

The primary design parameters for the trailing edge blowing geometry included:

- Number of blowing holes in the trailing edge array
- Individual hole diameters
- Chord-wise location of the blowing hole array
- Blowing hole angle relative to the blade exit angle, α_2

Park and Cimbala (1991) and Naumann (1992) both showed the importance of the trailing edge blowing geometry on wake attenuation characteristics. In general, blowing geometries that produce the most mixing will yield better wake attenuation. For best mixing, Naumann showed the superiority of discrete blowing jets over continuous slots. Also, in applications in which the flow is turned, such as the current IGV cascade, Sell (1997) showed the importance of orienting the blowing jets with the actual exit angle of the flow (deviation angle) rather than the blade exit angle (metal angle). For manufacturing concerns, only a single row of blowing holes was employed. Although Park and Cimbala's results indicated that a single row of blowing might result in longer attenuation distances, this configuration also produces the narrowest wake.

Two trailing edge blowing designs were tested in this experiment: metal-angle blowing, which oriented the blowing jets very near to the blade exit angle, and deviation-angle blowing, which oriented the blowing jets at a significant deviation angle from the blade exit angle. Each blowing design contained one array of 14 blowing holes. The hole array consisted of 3/64-inch diameter holes equally spaced 0.08 inches from center to center. The metal-angle blowing holes protruded through the trailing edge of the blade at x/C = 1 and were angled approximately 1.5° up-pitch from the blade exit angle. The deviation-angle blowing holes protruded through the blade's suction surface at x/C = 0.96 and were angled toward the exit plane of the cascade with a 14° angle from the local blade surface. This corresponded to a jet deviation angle of approximately 9° from the blade exit angle. For both designs, the blowing hole array was centered on the blade

span, creating a one-inch flow control span behind the IGV with 2.5-inch spans of non-controlled wake on both ends of the IGV.

The amount of mass flow required for the trailing edge blowing was estimated from a momentum analysis. Ideally, one would like the momentum deficit of the blade wake to be completely replaced by the momentum of the trailing edge blowing jets. Using baseline probe data presented in Appendix A, the expected wake momentum deficit and required blowing jet momentum were estimated by the following relations:

$$\text{Wake momentum deficit} = \int \rho\, U_\infty^2\, dA - \int \rho\, u^2\, dA$$

$$= S_{teb}\left\{\int \rho\, (U_\infty^2 - u^2)\, dy\right\}$$

$$\text{TEB jet momentum} = \int \rho\, U_{jet}^2\, dA$$

$$= \rho\, U_{jet}^2\, n\, A_{jet}$$

where:

ρ = local density as calculated from local pressure and temperature data

U_∞ = free-stream flow velocity at the blade exit

u = local velocity at the blade exit as calculated from pressure data

S_{teb} = span of TEB flow control region

U_{jet} = estimated maximum velocity of TEB jet flow

n = number of TEB jets

A_{jet} = area of an individual TEB jet

The minimum trailing edge blowing mass flow required to completely replace the wake momentum deficit was estimated from baseline tunnel data and the above relations. Due to the constrictive nature of the trailing edge jet holes and the plenum supply tubes, the maximum velocity attainable by the TEB jets was estimated assuming adiabatic flow with friction (Fanno

flow). According to the Fanno flow estimates, the maximum mass flow attainable by the trailing edge blowing design corresponded to an estimated 42% wake momentum deficit replacement.

The suction and blowing configurations described in Sections 2.2.2 and 2.2.3 resulted from low-speed tests performed in front of a centrifugal blower and preliminary wind tunnel traverse measurements. Appendix A describes the blower setup and test results and presents preliminary wind tunnel test results used in the refinement of the flow control design.

Figure 2.4 shows a cross-sectional drawing of the flow control blade with the metal-angle blowing, and Figure 2.5 shows a cross-sectional drawing of the flow control blade with the deviation-angle blowing. Important features of both the boundary layer suction and trailing edge blowing designs are labeled in these figures.

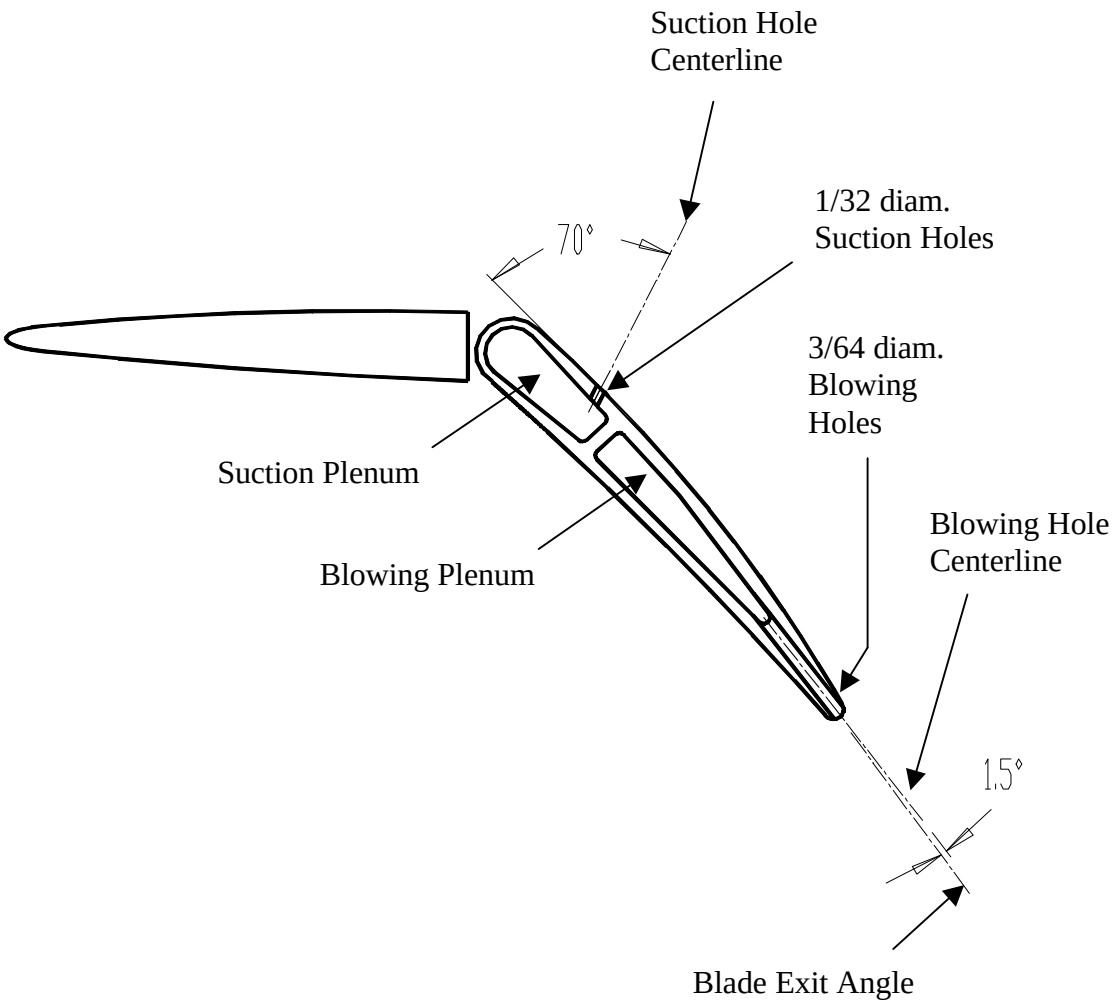

Figure 2.4 Flow Control Blade Cross-Section, Metal Angle Blowing design

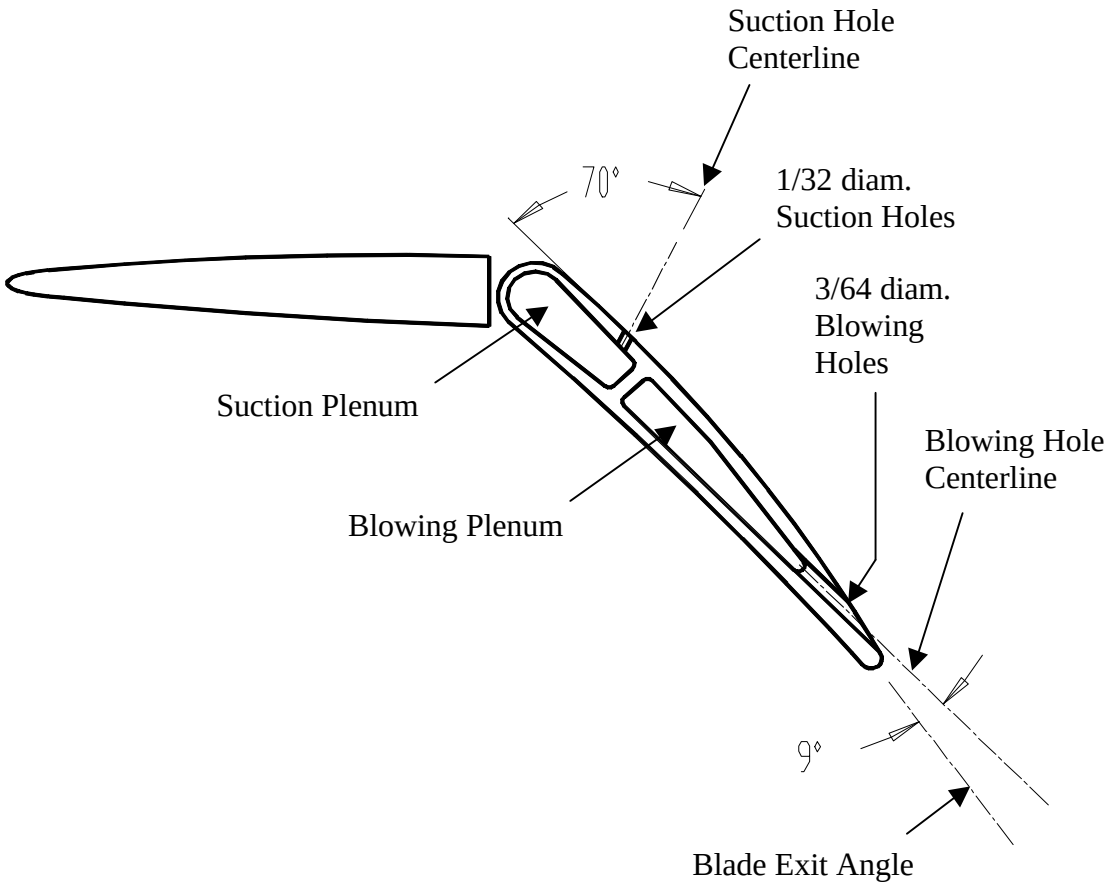

Figure 2.5 Flow Control Blade Cross-Section, Deviation Blowing design

2.3 The Wind Tunnel Facility

The IGV cascade was tested in the Virginia Tech transonic wind tunnel. The transonic wind tunnel is a blow-down type facility. The air to the wind tunnel is supplied by two storage tanks which are pressurized by a four stage, reciprocating compressor. Upon discharge from the storage tanks, the air is cooled and passed through an activated-alumina dryer to dehumidify the air before entering the wind tunnel. A pneumatically controlled butterfly-type control valve is used to maintain a constant inlet total pressure to the test section. A personal computer is used to supply a voltage signal to an electro-pneumatic converter that produces a proportionate output pressure based on the input voltage from the computer. The voltage signal from the computer is described by seven constants. One of those constants, the objective inlet total pressure, is modified to produce different inlet Mach numbers to the test section. The flow coming from the control valve passes through a flow straightener and a meshed wire frame to provide uniform flow to the test section. The flow exits the test section through an exhaust duct, and then passes through a muffler before exiting to the atmosphere outside of the lab facility. Figure 2.6 shows the structure of the transonic wind tunnel.

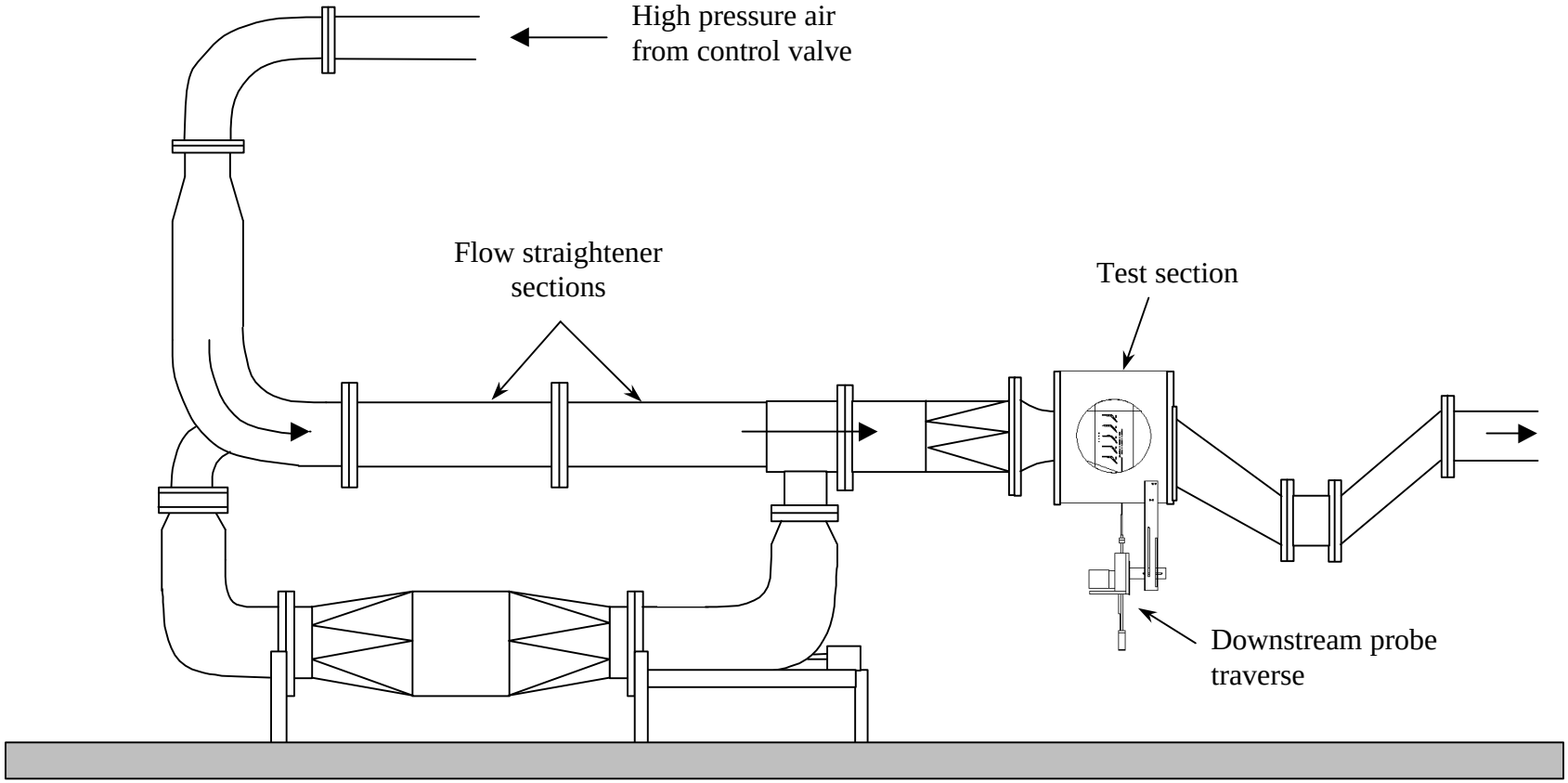

Figure 2.6 Virginia Tech Transonic Wind Tunnel

The test section is constructed from an aluminum frame with openings in the sides for the cascade. The top and bottom of the flow region are formed by the top and bottom aluminum blocks of the test section. The top and bottom blocks each have 0° entry and 22° exit angles. The cascade Plexiglass and the aluminum retainers that hold the cascade within the test section form the sides of the flow region. The retainers support the Plexiglass such that the blades are visible from both sides of the assembled test section. This allows for the use of optics-based flow visualization. The bottom block of the test section has a smaller, removable aluminum block with an opening for a downstream probe. This block can be replaced to allow for different streamwise probe locations or probe angles.

2.4 Flow Control Setup

The boundary layer suction supply tubes were connected to a common manifold by flexible Teflon tubing. A Vaccon VDF-500 ejector pump supplied the vacuum source for the suction manifold. The vacuum pressure of the pump could be adjusted to provide various suction flowrates. It was capable of providing a maximum sustained vacuum pressure of approximately –9.6 psig. A filter, Meriam Instrument Laminar Flow Element, thermocouple, and two pressure transducers were placed inline with the manifold and pump to measure the mass flow rate of the air removed through the boundary layer suction holes. The ejector pump required an 80 psig air source to generate the vacuum flow.

The trailing edge blowing supply tubes were connected to a common manifold by flexible Nylon tubing. The blowing manifold was connected to the same high-pressure source as the motive air for the ejector pump. A fixture containing three differently sized orifice plates, connected in parallel, was placed inline with the manifold to allow for measurement of a wide range of blowing mass flow rates.

The high-pressure source for both the ejector pump and the trailing edge blowing manifold was a large pressure tank within the tunnel facility. This tank was pressurized by a single stage reciprocating compressor. The compressor was feedback-controlled to maintain a constant tank pressure of 150 psig. There were two outlets from the pressure tank, both of which were fitted

with pressure regulators. One regulator was set to an output pressure of 80 psig and connected to the ejector pump high-pressure input. The second regulator was connected to the inlet of the orifice fixture. Its output pressure was modified depending on the desired trailing edge blowing mass flow. Figure 2.7 shows a schematic of the flow control setup.

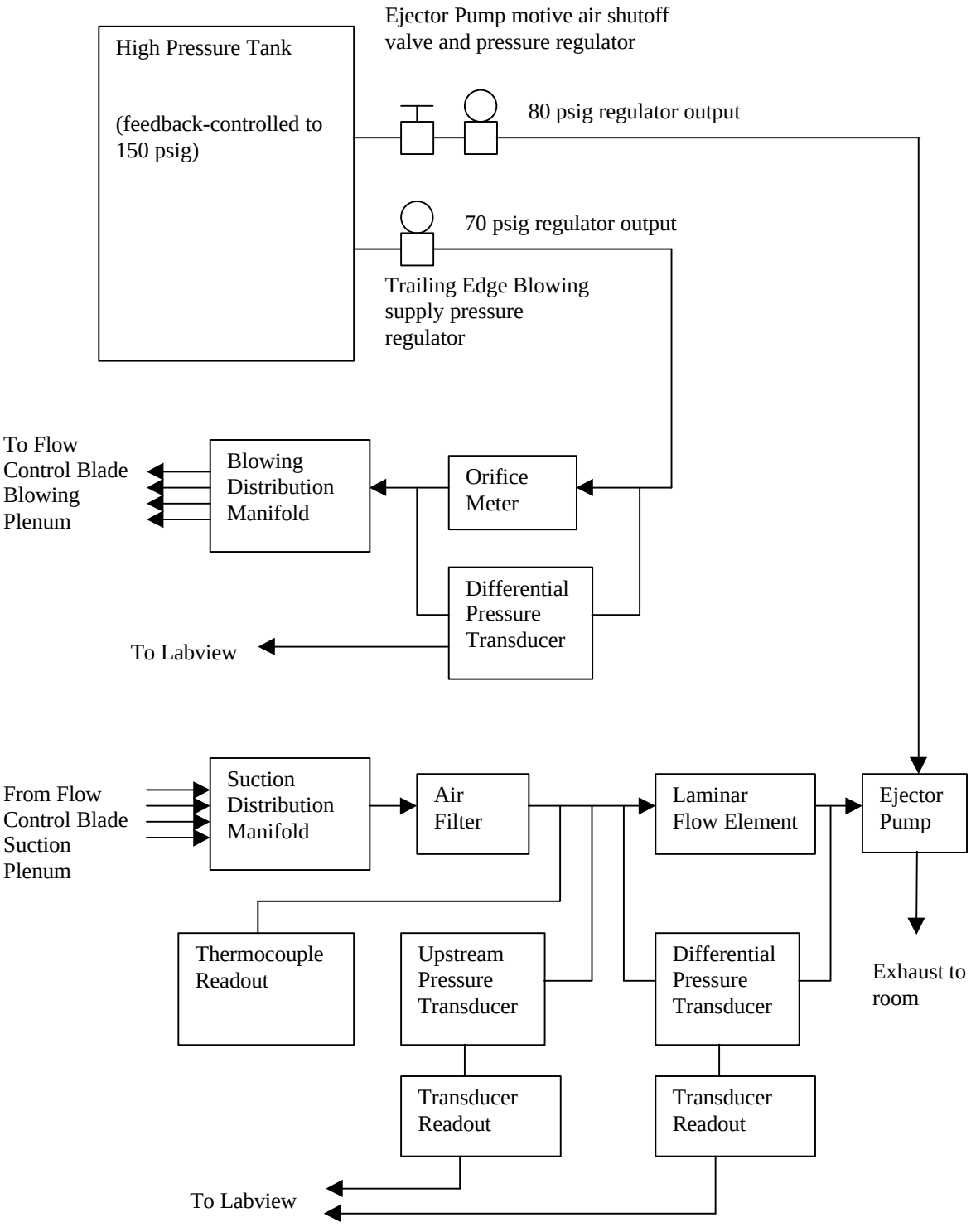

Figure 2.7 Schematic of Flow Control Equipment Setup

2.5 Instrumentation and Data Acquisition

The losses through the cascade were quantified completely from aerodynamic measurements. Aerodynamic measurements used for calculating losses included:

- Upstream total pressure
- Upstream static pressure
- Upstream total temperature
- Downstream static pressure
- Differential total pressure between upstream and downstream conditions

The upstream total pressure, P_{t1}, was measured with a stationary Pitot probe positioned approximately one foot ahead of the test section. This Pitot probe was connected to a single channel pressure transducer capable of measuring from 0 to 100 psig. The pressure transducer, which produces a linear 0 to 6 VDC output over its full scale, was calibrated with an AMETEK deadweight tester. The deadweights are categorized in terms of gage pressure. Calibration consisted of obtaining voltage outputs from the transducer for known input pressures applied by the deadweight tester. Calibration data points were taken from 0 to 10 psig in 1 psig increments.

The upstream total temperature, T_{t1}, was measured with an OMEGA type K thermocouple. This thermocouple was located at approximately the same position as the P_{t1} Pitot probe. The output from the thermocouple was directly converted to degrees Centigrade by the data acquisition software.

Both the upstream and downstream static pressures, P_1 and P_2, were measured with static taps through the cascade's Plexiglass sidewalls. The sidewall static pressure taps are labeled in Figure 2.2. All of the static pressure taps were 1/32-inch in diameter. There were a total of four upstream taps. They were located 19% chord in the streamwise direction ahead of the leading edge of the front tandem and spaced 24% pitch apart. The upstream taps measured pitch-wise static pressures entering the second and third passages. There were a total of 19 downstream taps. They were located 28% chord in the streamwise direction behind the trailing edge of the back tandem and spaced 12% pitch apart. The downstream taps measured pitch-wise static

pressures exiting the second and third passages. Both the second and third blade passages contained eight downstream static pressure taps.

The static pressures were recorded using an independent, self-calibrating Pressure Systems, Incorporated (PSI) Model 780C pressure scanning system. The PSI is controlled by a personal computer and is capable of reading 32 channels from the pressure scanner. The downstream taps were connected to channels 1 through 19, with the uppermost downstream tap as tap #1. The upstream taps were connected to channels 22 through 25 with the uppermost upstream tap as tap #22. The PSI math processor processes the voltage signals returned by the pressure scanner, and data is written to the control computer directly in gage pressure. For this experiment, the PSI was set to scan the downstream pressures for fifteen seconds. During the scan period, the PSI recorded fourteen static pressures, each of which was an average of ten measurements, for each tap.

The differential pressure between upstream total conditions and downstream total conditions was measured with a traversing total pressure probe. The probe tip was angled to closely match the blade exit angle of the back tandem, and it traveled in a pitch-wise motion parallel to the exit plane of the IGV cascade. The tip of the probe was located at the same streamwise location as the downstream static pressure taps. A Rapidsyn stepper motor controlled the probe traverse movement. The traverse motor, which was controlled by a personal computer, was programmed to traverse the probe approximately 2-1/2 blade passages, starting at the same pitch location as static tap #1. The position of the probe was measured with an LVDT transducer attached to the probe traverse assembly. The LVDT had a linear output from –3 to +3 VDC. The pressure line from the traverse probe was connected to an MKS differential pressure (DP) transducer. The reference-pressure input to the DP transducer was teed into the pressure input of the P_{t1} transducer. The DP transducer had a 0 to 3 psid range over a 0 to 3 VDC full-scale voltage output. The calibration of this sensor was verified using the deadweight tester.

The boundary layer suction mass flow was measured using a Meriam Instrument Laminar Flow Element (LFE). A Validyne pressure transducer, calibrated to read pressure in inches of water, measured the differential pressure across the LFE. Another Validyne pressure transducer,

calibrated to read pressure in psig, measured the line pressure upstream of the LFE. An Omega Type K thermocouple measured the upstream air temperature in degrees centigrade.

The trailing edge blowing mass flow was measured with a 0.180-inch diameter Lambda Square orifice meter. The differential pressure across the orifice meter was measured using a Validyne DP transducer calibrated to read pressure in psig. An Omega Type K thermocouple was used to measure the upstream air temperature in degrees Centigrade, and an analog gage was used to measure the upstream line pressure in psig.

The voltage outputs from many of the pressure and temperature sensors were recorded using a Labview-based data acquisition system. The Labview data acquisition system consisted of a personal computer and a multiplexor capable of recording 32 voltage signals and 32 thermocouple signals. The sampling frequency and the number of samples to be recorded per channel were user defined. The data acquisition board in the Labview computer had a built-in filter to reduce signal noise. For this experiment, data was sampled at 100 Hz, and 1400 samples per channel were recorded. This resulted in a 14 second run time. The signals acquired by Labview included:

- Upstream total pressure
- Differential pressure
- Traverse probe position
- Orifice differential pressure
- LFE differential pressure
- LFE upstream pressure
- Upstream total temperature

The LFE upstream temperature was recorded manually. The orifice meter upstream pressure and temperature were also recorded manually. A schematic of the data acquisition system appears in Figure 2.8.

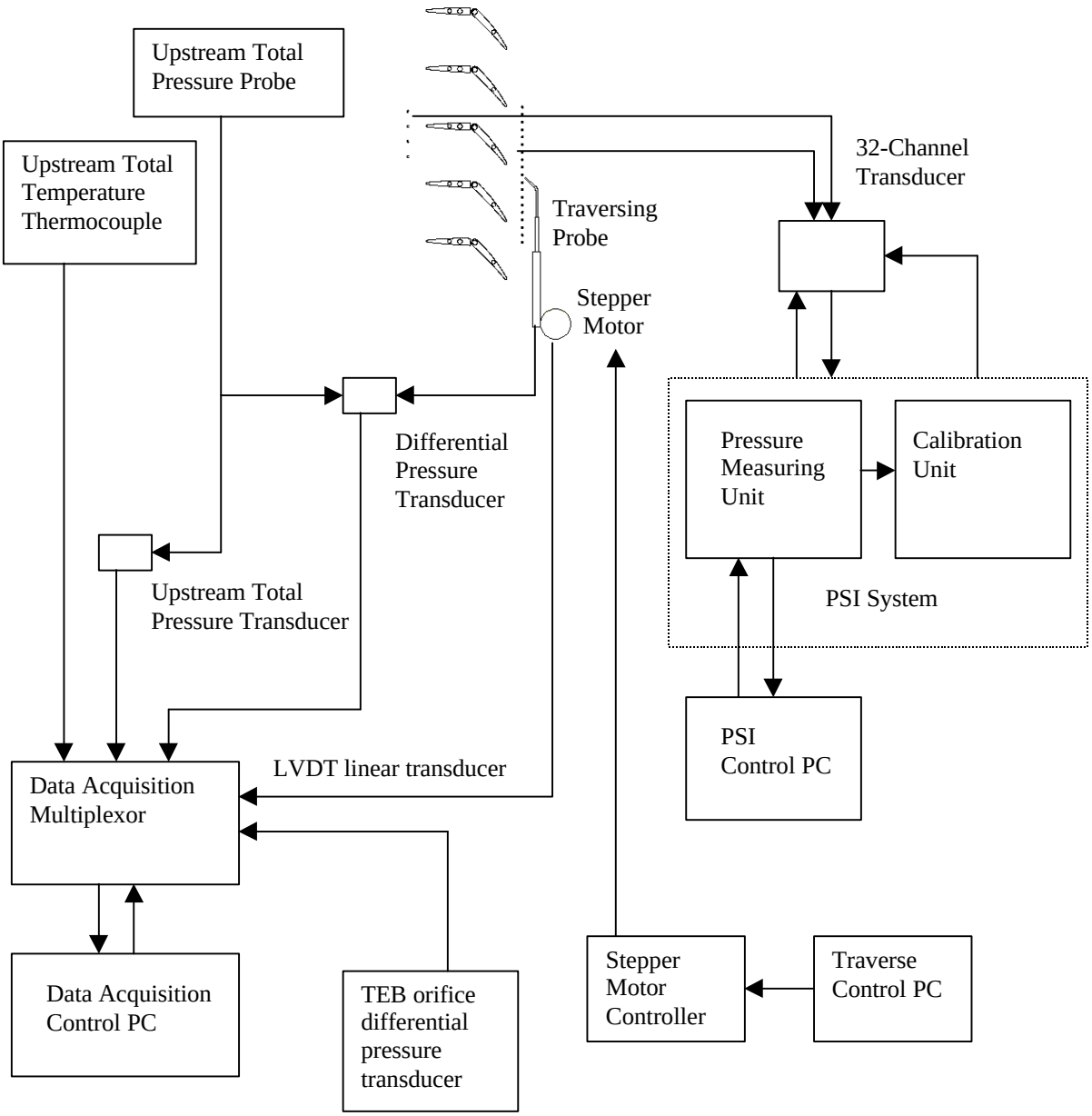

Figure 2.8 Schematic of Data Acquisition System

2.6 Flow Visualization

In order to gain a qualitative understanding of the baseline flow, two flow visualization techniques were used: Schlieren photography and Colored surface oil flow visualization.

2.6.1 Schlieren photography

Schlieren photography is an optical technique for visualizing the flow of gases. The Schlieren setup used in this experiment, shown in Figure 2.9, was a two-mirror system. The brightness of an image formed by the Schlieren setup depends upon differences in the gradients of the refractive index in the light path. The Schlieren field of flow through the cascade is reproduced in various tones on the film. Opaque objects, such as the IGV's and the cascade retainers, appear in silhouette. Schlieren methods are sensitive enough to detect temperature differences as small as 10° Fahrenheit. They are very useful in visualizing flow phenomenon such as separation, turbulence, and shock waves. For this experiment, Schlieren photography was used to qualitatively visualize the severity of the suction surface separation on the back tandems, flow periodicity, and wake width.

2.6.2 Colored surface oil flow visualization

Surface oil flow visualization involves coating the blade surfaces and the Plexiglass sidewalls with contrasting fluorescent colors. The cascade is installed in the wind tunnel, and the wind tunnel is run at the same condition as when taking the aerodynamic measurements. The patterns formed on the blades and sidewalls are used to interpret flow behavior, such as flow separation, secondary flows, and shock location. For this experiment, the surface oil flow visualization was used to identify the location and severity of the suction surface separation on the back tandem.

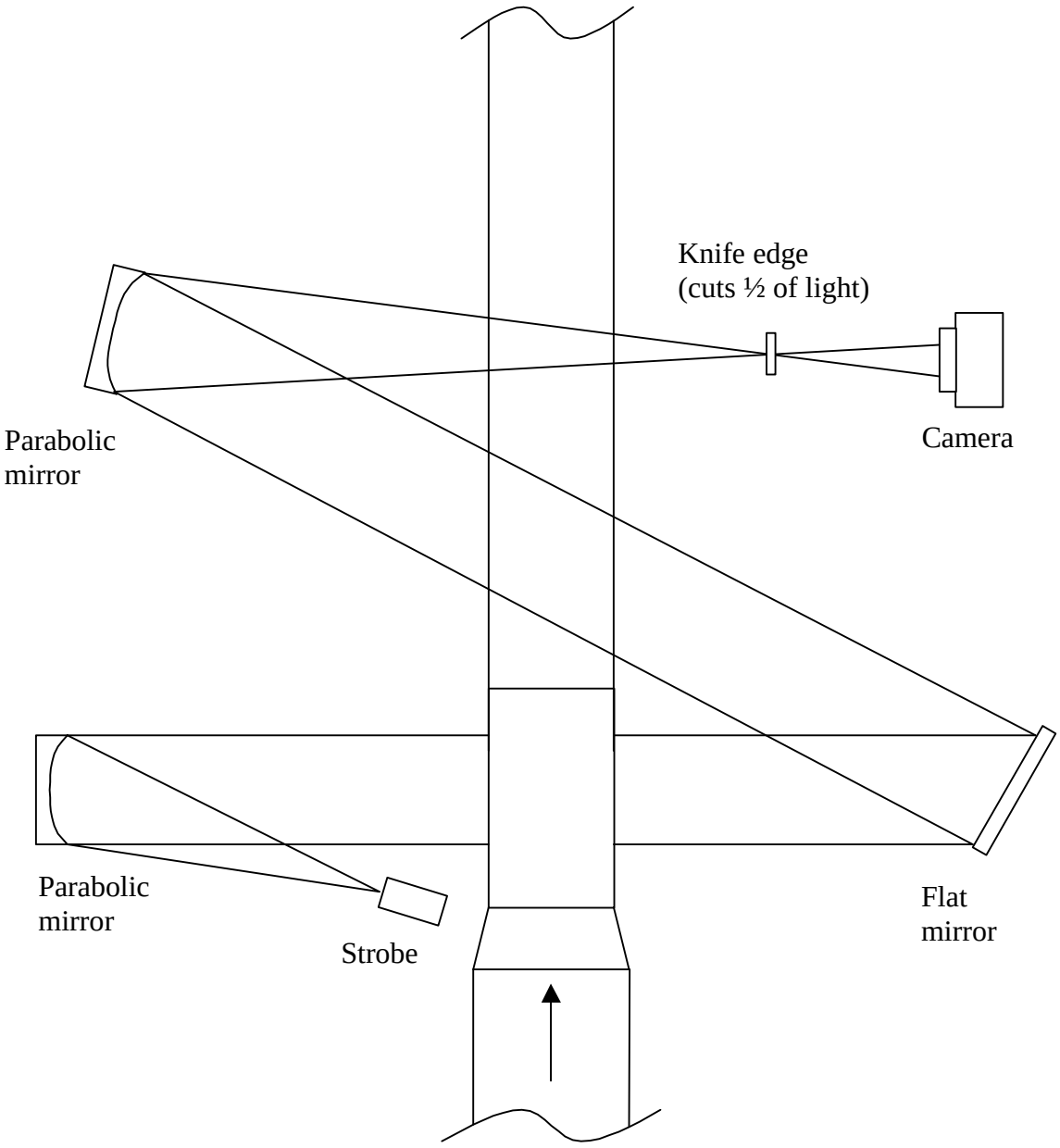

Figure 2.9 Two-Mirror Schlieren Photography Setup

2.7 Data Reduction

Two major parameters were used to measure the effectiveness of the flow control: pressure loss coefficient, and wake momentum deficit.

2.7.1 Pressure Loss Coefficient

There are many common forms for expressing the pressure loss across a blade cascade. The loss coefficient calculated in this experiment was the area-averaged stagnation pressure loss as defined for a turbine blade passage. This equation is displayed in equation 2.7.1:

$$w = \left[\frac{\int_{mid-passage}^{mid-passage} \left\{ \left(P_{t,1} - P_{t,2} \right) / P_{t,1} \right\} dy}{\int_{mid-passage}^{mid-passage} dy} \right] \qquad (2.7.1)$$

In discreet form, equation 2.7.1 becomes:

$$w = \frac{\sum_{i-1}^{n} \left\{ \left(P_{t,1i} - P_{t,2i} \right) / P_{t,1i} \right\} \Delta y}{y_n - y_1} = \frac{\sum_{i=1}^{n} \left\{ DP_i / P_{t,1i} \right\} \Delta y}{y_n - y_1} \qquad (2.7.2)$$

In equation 2.7.2, each i index corresponds to the i-th P and y values. The starting point, at i = 1, was set at a pitch location of 0.4. The end point, at i = n, was set at a pitch location of 1.4. Blade #2, the blade immediately above the flow control blade, was assigned as the zero pitch reference. Figure 2.10 shows the pitch scale used in all of the data analysis. The loss coefficient was calculated in this manner in order to capture the full effects of the flow control since flow control was only applied to one blade and hence only one wake. The acquired P_t, DP, and position voltage signals were converted to pressures and position for use in the above equations using the previously constructed calibration curves.

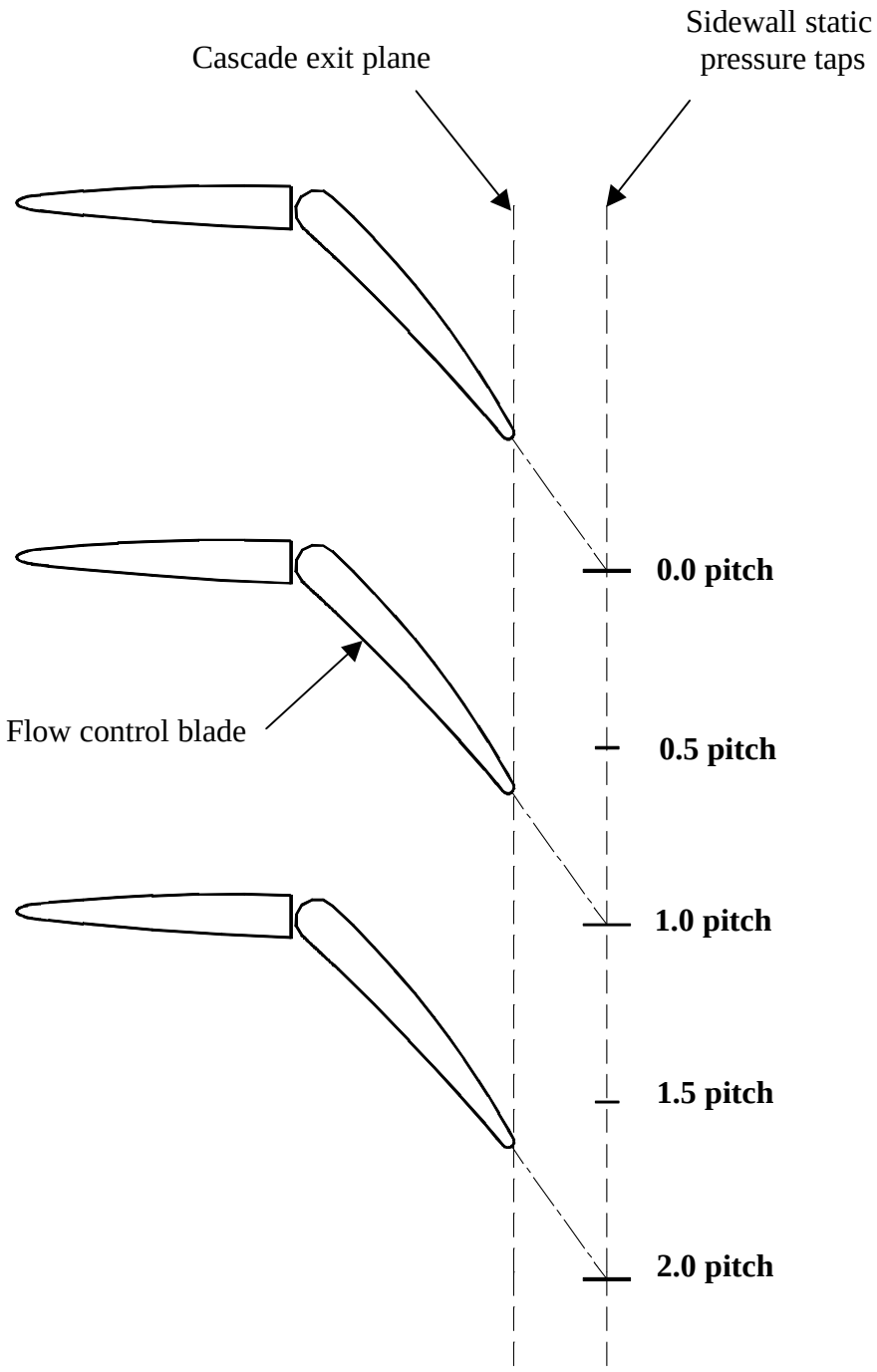

Figure 2.10 Cascade Pitch Scale

2.7.2 Wake Momentum Deficit

For easy comparison with results from experiments described in Chapter 1, wake momentum deficits were expressed in terms of the dimensionless wake momentum thickness, θ/d, as follows:

$$\frac{q}{d} = \int_{mid-passage}^{mid-passage} \frac{u}{U_\infty}\left(1 - \frac{u}{U_\infty}\right) d\left(\frac{y}{d}\right) \qquad (2.7.3)$$

In equation 2.7.3, d is the maximum thickness of the back tandem, 0.230 inches. In discreet form, equation 2.7.3 becomes:

$$\frac{q}{d} = \frac{1}{d}\sum_{i=1}^{n} \frac{u}{U_\infty}\left(1 - \frac{u}{U_\infty}\right) \Delta y \qquad (2.7.4)$$

The i = 1 and i = n positions in equation 2.7.4 were identical to those assigned for equation 2.7.2. A wake momentum thickness of zero would correspond to a momentumless wake with no net momentum deficit or excess.

The local exit velocity, u_2, in equation 2.7.4 must be calculated from the measured pressure and temperature data. The exit velocity was calculated from the following equation:

$$u = M\sqrt{gRT} \qquad (2.7.5)$$

The exit Mach number was calculated from:

$$\frac{P_t}{P} = \left(1 + \frac{g-1}{2} M^2\right)^{\frac{g}{g-1}} \qquad (2.7.6)$$

Equation 2.7.6 required both static and total pressures at each y-position. While the total pressure was recorded at 464 positions by the traverse probe from the 0.4 to 1.4 pitch locations, only eight static pressure taps were located within this same pitch distance. In order to maintain good resolution for calculating the momentum thickness, the static pressure data was curve fit with straight lines connecting the values recorded at each tap. Static pressures corresponding to each total pressure measurement were then estimated using the piecewise curve fit.

Static temperatures were determined from the upstream total temperature using the following equation:

$$\frac{T_t}{T} = 1 + \frac{g - 1}{2} M^2 \qquad (2.7.7)$$

Equation 2.7.7 was applied to both the upstream and downstream conditions assuming that the total temperature remained constant through the cascade.

The air density at the entrance of the cascade, ρ_1, was required for calculating the mass flow through the blade passage. It was determined from the ideal gas law:

$$r_1 = \frac{P_1}{RT_1} \qquad (2.7.8)$$

Equations 2.7.5 through 2.7.8 were applied at each data point from the start of the probe traverse movement to the end of the probe traverse movement. After converting the traverse position curve to pitch, Equations 2.7.2 and 2.7.4 were applied from 0.4 pitch to 1.4 pitch to calculate the loss coefficient and the wake momentum thickness.

2.7.3 Boundary Layer Suction and Trailing Edge Blowing Mass Flows

The mass flow removed by the boundary layer suction, which was measured by the LFE, was calculated from a calibration equation supplied by the manufacturer. The general calibration equation for this series of LFE is:

$$ACFM = [B*DP+(C*DP^2)]*0.9885 \qquad (2.7.9)$$

In equation 2.7.9, ACFM is the actual volumetric flow rate measured by the LFE in cubic feet per minute, DP is the differential pressure across the LFE in inches of water, and B and C are calibration constants unique to each LFE. B and C were determined by the manufacturer. For Virginia Tech's LFE, B = 12.9703 and C = -0.0617892. The volumetric flowrate was multiplied by the upstream air density in the LFE line to obtain the mass flow removed by the boundary layer suction. The air density was determined from the upstream static temperature and pressure using equation 2.7.8.

The mass flow injected by the trailing edge blowing, which was measured by the orifice meter, was calculated from the following equation:

$$\dot{m} = C_d A \sqrt{2 r \Delta P} \sqrt{\frac{1}{1-b^4}} \qquad (2.7.10)$$

For the 0.180 inch diameter orifice meter used in this experiment, $C_d = 0.61$, and $\beta = 0.4186$. The upstream density of the blowing air was determined from the upstream static temperature and pressure using equation 2.7.8.

Chapter 3.0 EXPERIMENTAL RESULTS AND DISCUSSION

Results have been obtained to show that boundary layer suction was effective at reducing the pressure loss coefficient and the wake momentum thickness with a relatively small penalty. The addition of metal-angle blowing proved to be effective at further reducing these quantities. A large mass flow addition was required in order for metal-angle blowing to be effective. The addition of deviation-angle blowing in place of the metal-angle blowing proved to be ineffective at reducing either the loss coefficient or the wake momentum thickness.

The following sections describe in detail the results for each of the test cases. The flow conditions were held constant within the capabilities of the wind tunnel controls. The flap of the IGV was set at the 55.0° exit angle position. The inlet Mach number, M_1, was approximately 0.3, which corresponded to an inlet total pressure of approximately 2.6 psig. For all experiments, the Reynolds number based on the overall IGV chord length was greater than 500,000, thus ensuring Reynolds number independent cascade behavior (Sell, 1997).

3.1 Baseline

Data from several tunnel runs with no flow control was acquired to qualitatively and quantitatively understand the baseline flow. This data included surface oil flow visualization, Schlieren photography, and aerodynamic measurements acquired from the traverse probe.

The surface oil flow visualization and Schlieren photographs, shown in Figures 3.1 and 3.2, showed evidence of significant suction surface flow separation that appeared to begin near the leading edge of the IGV flap. The flow does not appear to reattach to the blade surface before exiting the cascade, resulting in the wide wakes seen in Figure 3.2. Quantification of the baseline flow separation was acquired from the aerodynamic data. The traverse probe measured the total pressure profile near the exit plane of the cascade. The profile was normalized with the upstream total pressure to obtain a pressure ratio, which was plotted against a percent-pitch scale (probe position divided by the blade pitch). Total pressure ratio profiles from each baseline run appear in Figure 3.3. It can be seen from this figure that the wake profiles were not symmetric

about the wake center. The non-symmetric wakes were further evidence of the flow separation seen in Figure 3.2. The center of the flow control wake was located at 0.86-pitch, which was farther up-pitch than the ideal-flow pitch location of 1.0. This was due to the flow separation and also to flow deviation from the ideal case of flow following the blade metal angle.

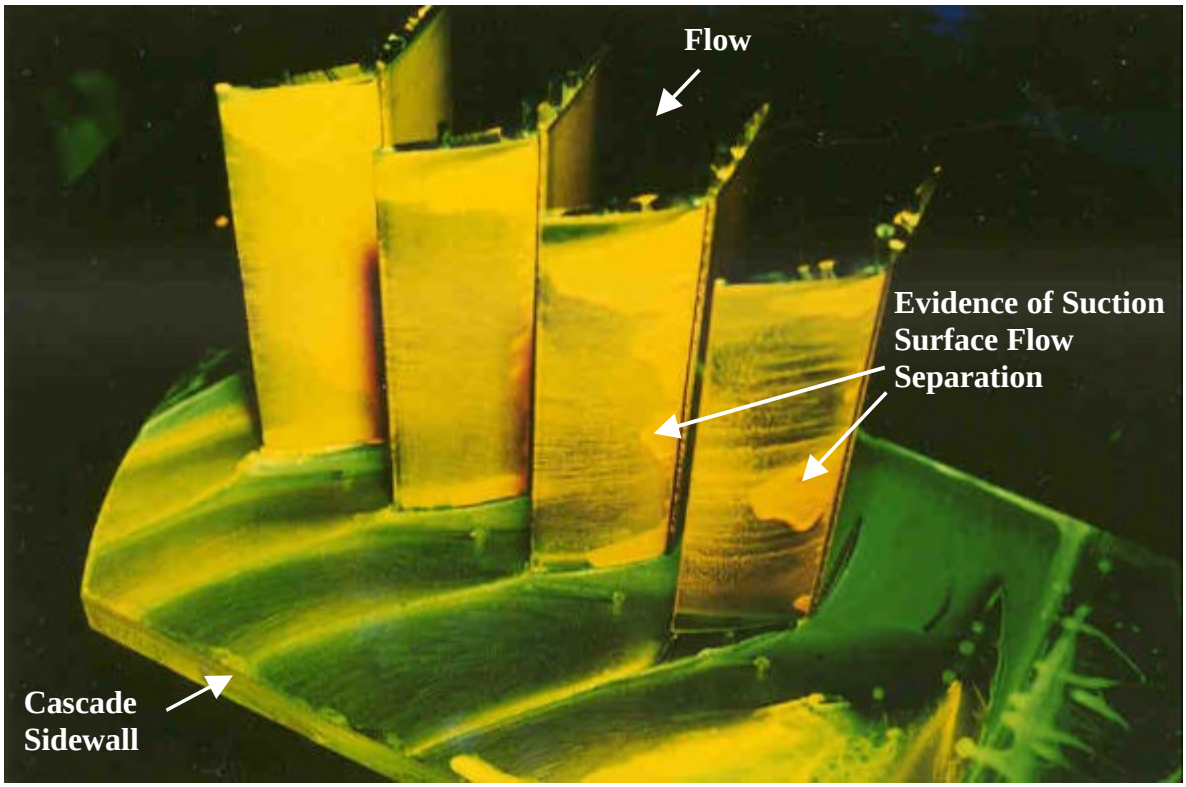

Figure 3.1 Surface Oil Flow Visualization of Baseline Flow (Blades 2, 3, 4, and 5 shown)

No Tunnel Flow

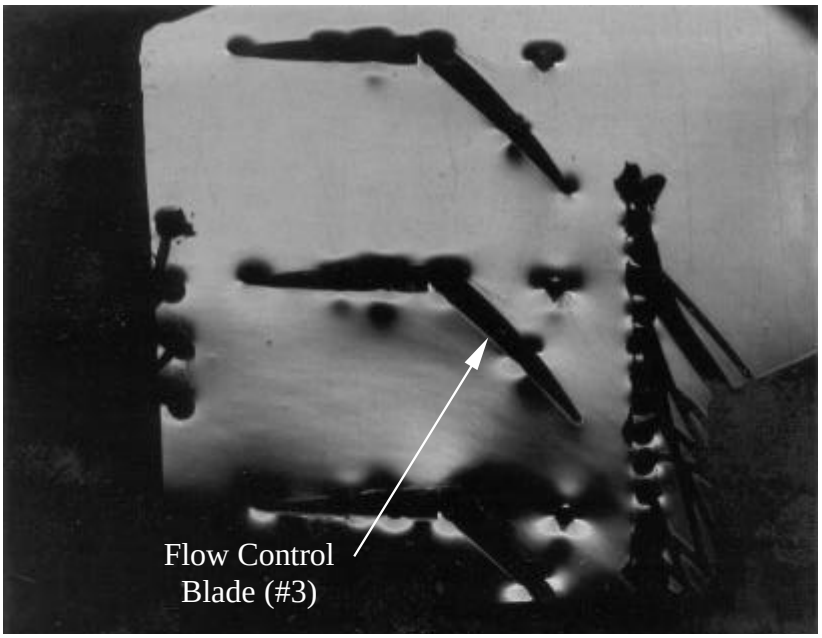

Inlet Mach Number = 0.3

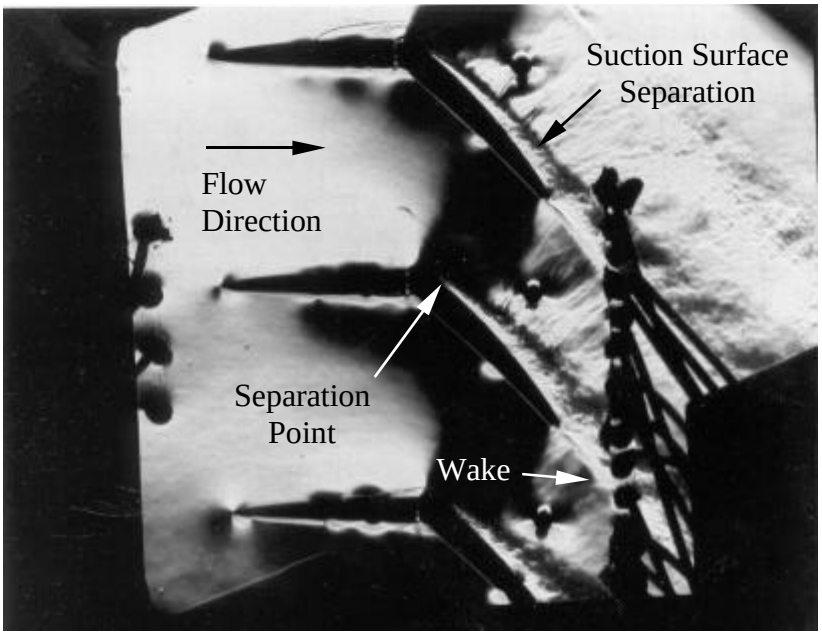

Figure 3.2 Schlieren Photograph of Baseline Flow (Blades 2, 3, and 4 shown)

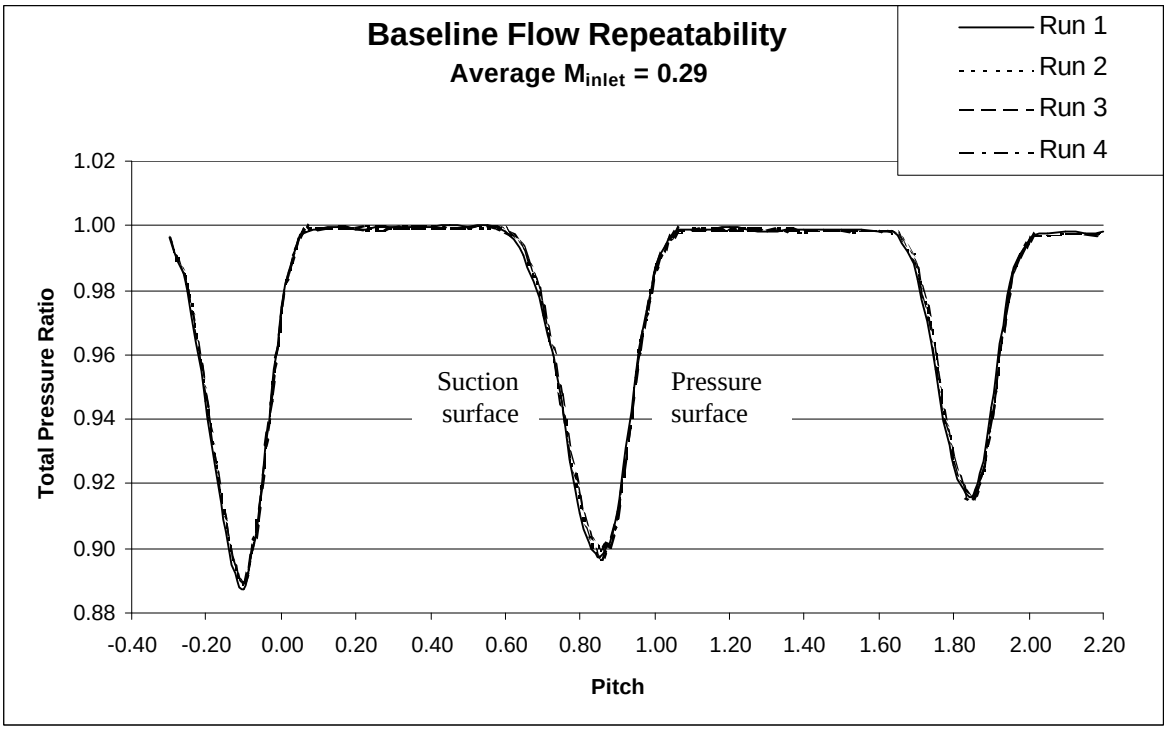

Figure 3.3 Baseline Flow Repeatability, Metal-Angle Blade

The periodicity of the flow in Figure 3.3 was less than ideal. The wake depths become successively smaller behind blades two, three, and four (minimum pressure ratios of approximately 0.90, 0.91, and 0.925, respectively). The non-periodic exit flow was attributed to the geometry of the test section relative to the cascade. The blade exit angle of the IGV was 55.0° while the angle of the tunnel floor and exhaust duct were only 22°. Hence, the cascade turned the flow into the floor of the test section. This blockage near the bottom of the cascade caused the flow exiting from the lower blade passages to slow down. Figure 3.4 shows profiles of the static pressures as measured by the sidewall taps for the four baseline runs. While the static pressure profiles show good repeatability, they also show a trend of steadily increasing static pressures from the top of the cascade to the bottom. The higher static pressures near the bottom of the cascade, even in the core flow regions between wakes, is consistent with the slowing of the flow as it was directed into the tunnel floor. The slower flow also resulted in

lower blade losses, accounting for the decreasing total pressure loss from the uppermost blade wake to the lowermost.

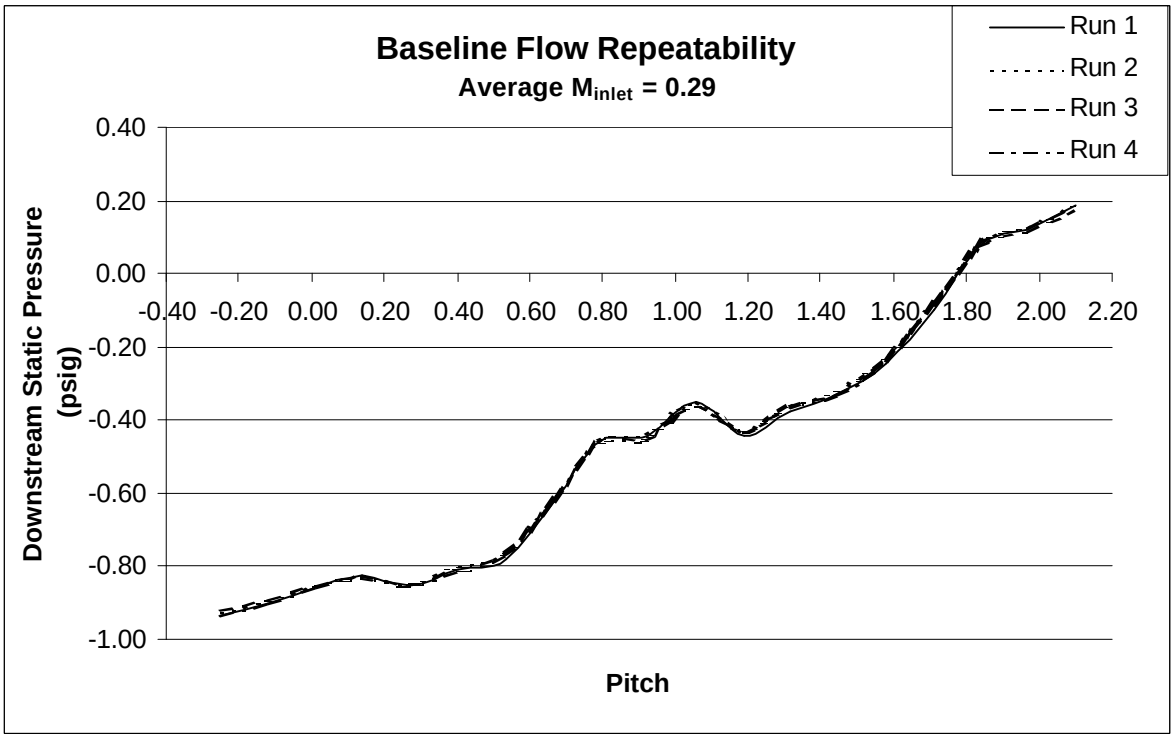

Figure 3.4 Static Pressure Profiles of Baseline Flow, Metal-Angle Blade

Although the non-periodicity was not desirable, the high repeatability of the flow made these results acceptable for achieving the goals of this experiment, which were to compare the flow control against the baseline flow for one blade passage.

The total pressure profile, along with the sidewall tap measurements, were used to construct exit Mach number profiles. Comparisons of the exit Mach number profiles from each run, as shown in Figure 3.5, also show good repeatability, but the periodicity is very poor. The poor exit Mach number periodicity was due to the poor total and static pressure periodicity shown in Figures 3.3 and 3.4. The steadily-decreasing core flow Mach number lead to difficulties when calculating the wake momentum deficit since U_∞ was determined from the exit Mach number. For

calculation purposes, M_∞, from which U_∞ was derived, was defined by a straight line connecting the local exit Mach numbers at the endpoints of the momentum integration interval rather than by a unique value, as illustrated in Figure 3.6. Unlike much of the previous research, the IGV's of the current experiment accelerated the flow, resulting in an average free stream exit Mach number of 0.53 for the flow control wake. The high exit Mach numbers created much larger wakes than what was observed at low exit Mach numbers (see Section 3.4 and Appendix A).

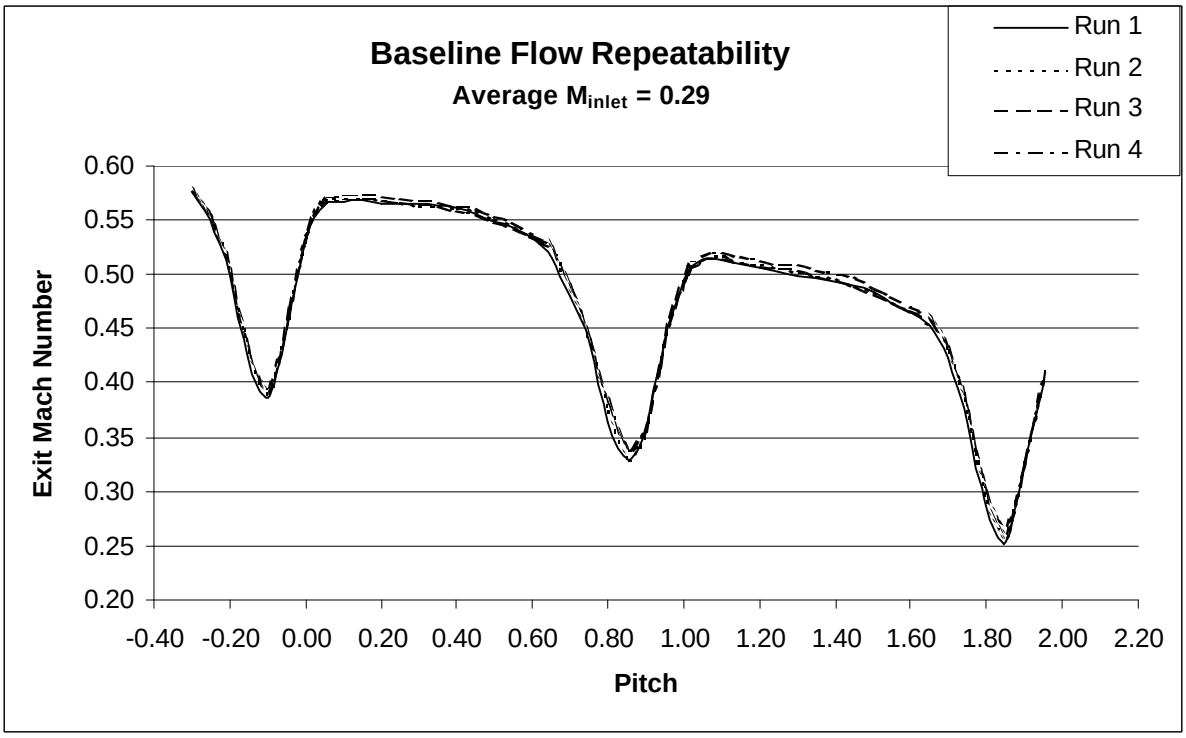

Figure 3.5 Exit Mach Number Profiles for Baseline Flow, Metal-Angle Blade

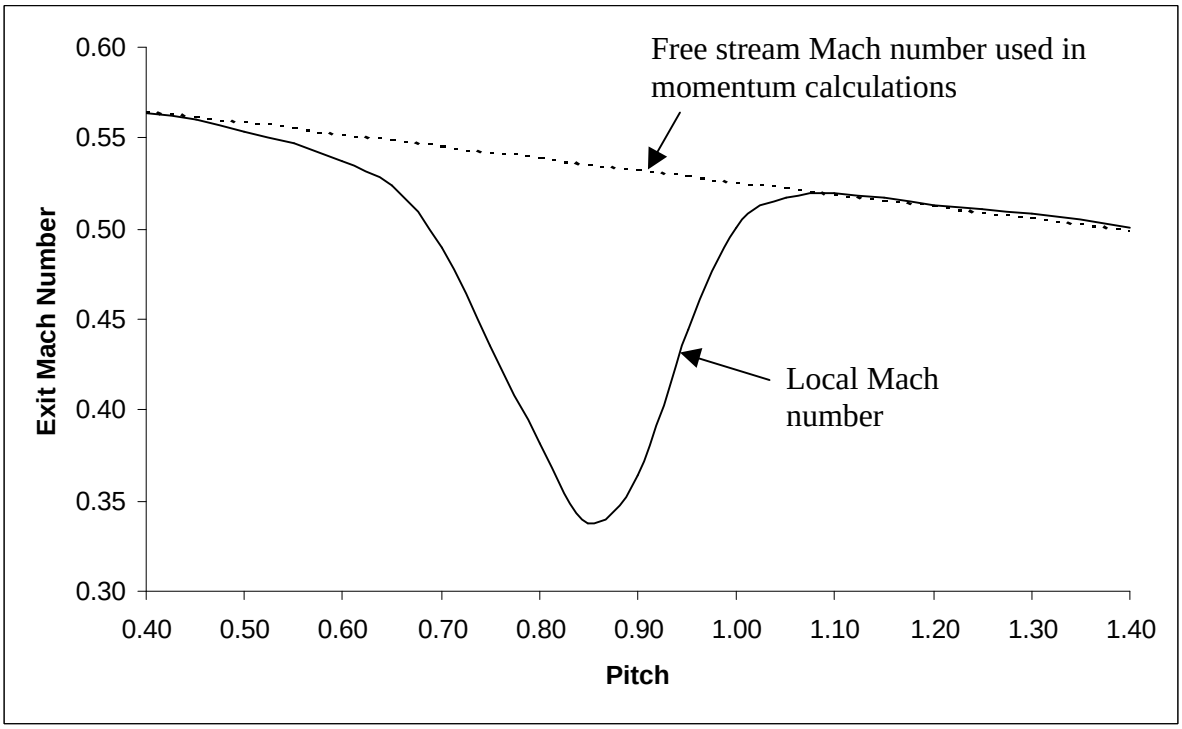

Figure 3.6 Definition of Free Stream Exit Mach Number

3.2 Flow Control: Metal-Angle Blowing

The first set of flow control experiments used the metal-angle blowing design shown in Figure 2.4. Figure 3.7 shows the total pressure ratio profiles of the flow control wake for the baseline, suction-only, and suction-plus-blowing tests. Figure 3.7 also includes error bars that indicate the uncertainty range of the pressure ratio profiles due to the slight variations between the repeatability runs.

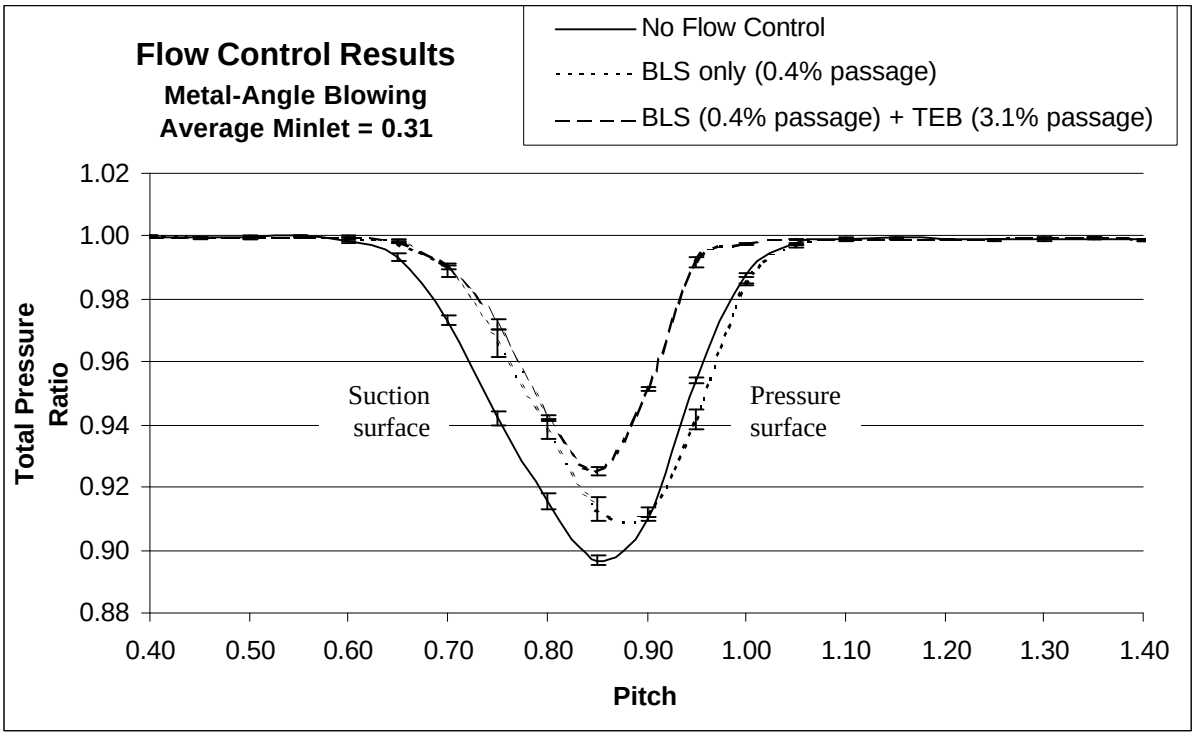

Figure 3.7 Comparison of Total Pressure Ratio Profiles for Flow Control Applied by Metal-Angle Blade Design

3.2.1 Boundary Layer Suction Only

For the suction-only case, the wake profile for the flow control blade was not symmetric about the wake center. However, it was more symmetric than the wake of the baseline flow. As seen in Figure 3.7, the onset of the flow control wake was delayed from 0.58-pitch to 0.64-pitch. This indicated that the boundary layer suction had successfully reduced the magnitude of the suction surface flow separation, resulting in the more even distribution of losses between the suction and pressure surfaces. The depth of the flow control wake with suction-only is clearly less than that of the baseline wake, and the wake center moved slightly down-pitch to 0.88-pitch. This also indicates a reduction in blade losses and provided further evidence of the reduced flow

separation. To obtain these results, the boundary layer suction removed 0.4% of the passage mass flow over the two-inch boundary layer suction span.

Three runs with suction-only were performed to verify the repeatability of the results. A comparison of the total pressure ratio profile for each suction-only run, as shown in Figure 3.8, shows good repeatability. The periodicity of the flow shows similar trends to that of the baseline runs for the same reasons described in Section 3.2.1.

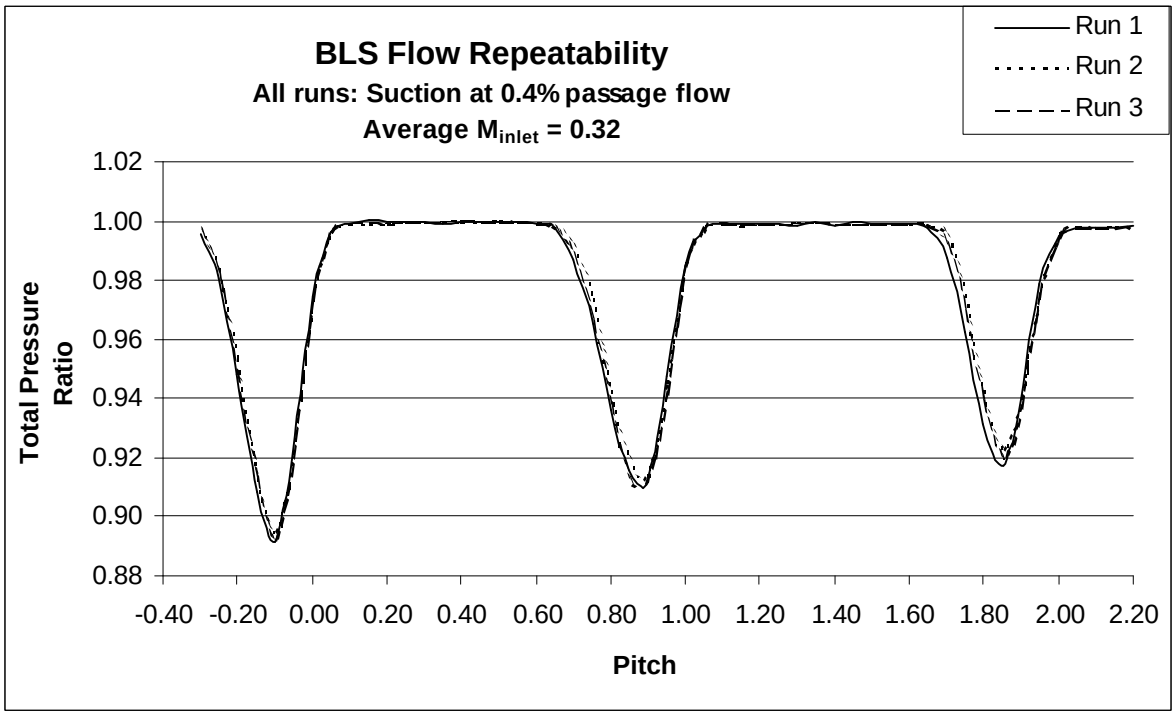

Figure 3.8 Suction-only Flow Repeatability, Metal-Angle Blade

3.2.2 Boundary Layer Suction Plus Trailing Edge Blowing

Figure 3.7 shows that the addition of metal-angle blowing caused the wake profile for the flow control blade to become less symmetric than when applying suction alone. The addition of the blowing did not, however, diminish any of the pressure loss reductions achieved by the boundary layer suction. This indicated that blowing near the metal angle of the blade had a greater effect on that portion of the wake attributed to the pressure surface viscous region. This result was consistent with the findings from the baseline experiments that showed significant flow deviation from the blade metal angle. The blowing configuration for this case directed the jet significantly down-pitch from the actual wake center. This can clearly be seen in Figure 3.9, which shows total pressure ratio profiles of the flow control wake for suction-only, suction-plus-blowing, and a probe traverse which measured only the metal-angle trailing edge blowing jets with no tunnel flow.

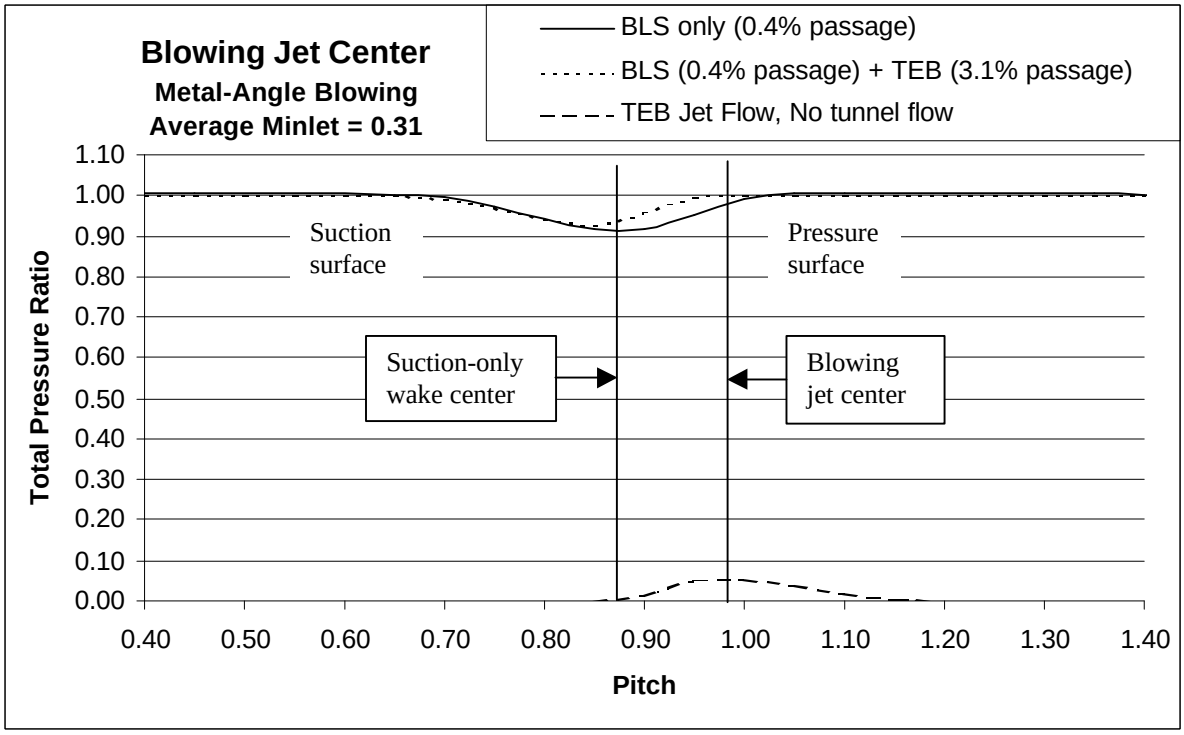

Figure 3.9 Blowing Jet Location for Metal-Angle blowing

The depth of the flow control wake with combined suction and blowing is clearly less than that of either the baseline or suction-only wakes, and the wake center moved farther up-pitch to 0.85-pitch. This indicated a further reduction in blade losses and provided evidence that some wake filling had been achieved by the metal-angle blowing. To obtain these results, the boundary layer suction removed 0.4% of the passage mass flow over the two-inch suction span, and the trailing edge blowing added 3.1% passage mass flow over the one-inch blowing span. The blowing manifold pressure was 70 psig.

Two additional runs using boundary layer suction in conjunction with trailing edge blowing were performed with blowing manifold pressures of 48 psig and 65 psig to examine the effects of different blowing flowrates. Figure 3.10 shows a comparison of the total pressure ratio profiles for the three blowing manifold pressures tested. As expected, increasing blowing manifold pressures, which increase the blowing mass flows, result in more wake filling and reduced total pressure losses. Due to limitations of the blowing setup, a blowing mass flow capable of creating a clearly visible jet peak in the total pressure ratio profile could not be obtained. Thus, a momentumless wake (one for which the momentum thickness integrates to zero) could not be achieved. However, as seen from the loss reduction obtained by the blowing in Figure 3.7, a momentumless wake achieved with the metal-angle blowing design would result in a large jet peak on the pressure side of the blade and a large wake peak on the suction side. Previous research has shown that blowing configurations that produce a symmetrical wake produce the lowest wake depths, widths, spreading rate, and achieve the greatest noise reduction (Park and Cimbala, 1991, Sell, 1997).

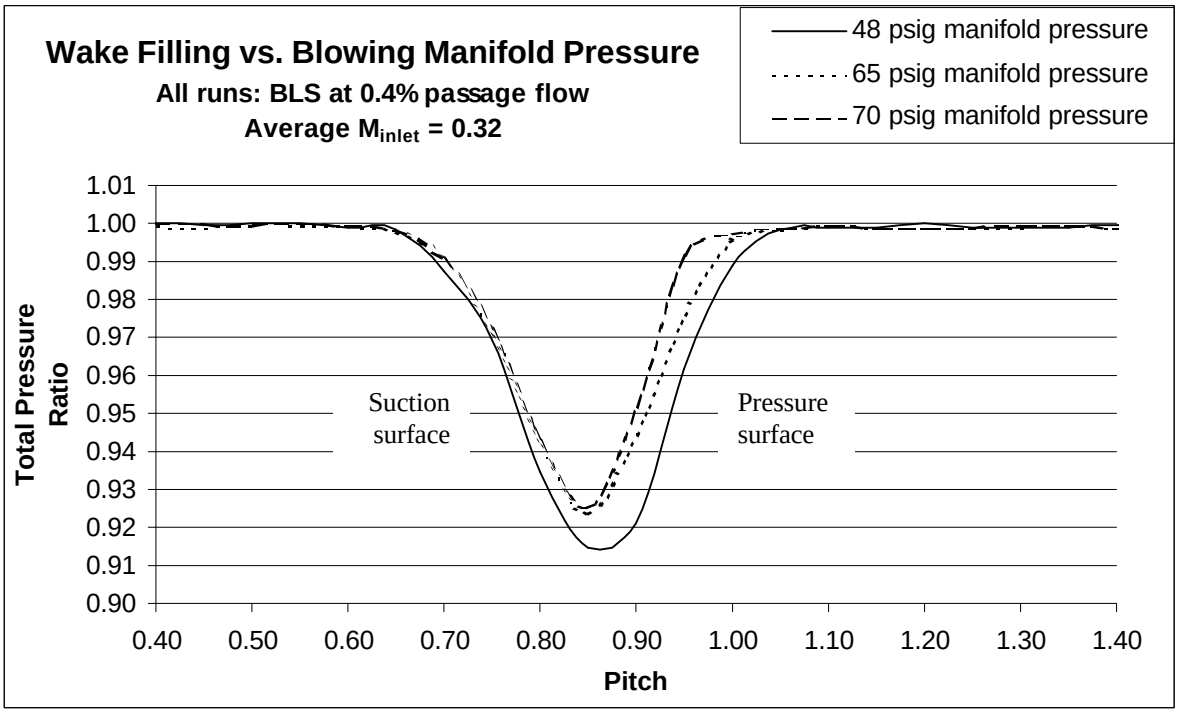

Figure 3.10 Comparison of Wake Filling with Suction + Metal-Angle Blowing at Multiple Blowing Manifold Pressures

Three runs with suction and metal-angle blowing at a manifold pressure of 70 psig were performed to verify the repeatability of the results. A comparison of the total pressure ratio profile for each run, as shown in Figure 3.11, shows good repeatability. The periodicity of the flow shows similar trends to that of the baseline runs for the same reasons described in Section 3.2.1.

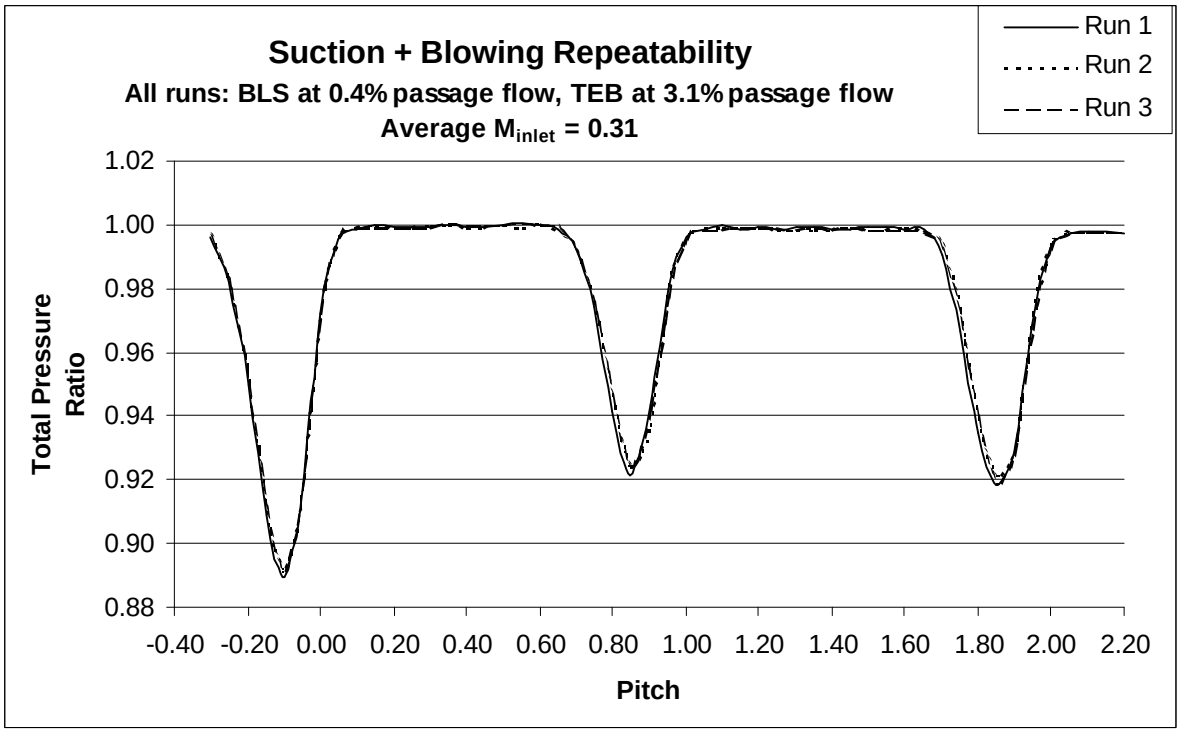

Figure 3.11 Suction + Metal-Angle Blowing Flow Repeatability

Table 3.1 summarizes the area-averaged pressure loss coefficient and wake momentum thickness results for the flow control tests performed with the metal-angle blowing design. The average inlet mach number was 0.31. The static pressure data for the 65 psig manifold pressure run was corrupt, hence a momentum thickness could not be calculated for this case. The percent reductions presented for both the loss coefficient and the wake momentum thickness are referenced to the baseline flow obtained during that tunnel entry. The uncertainty due to instrumentation accuracy is indicated below Table 3.1 for each result. The uncertainty analysis technique used to obtain the instrumentation error bound is presented in Appendix B.

Table 3.1

Loss Coefficient and Wake Momentum Thickness Reductions Achieved with Flow Control

Metal-Angle Trailing Edge Blowing Design

Case	Area-Avg'd. Loss Coeff.	Reduction of Loss Coeff.	Wake Momentum Thickness	Reduction of Wake Momentum Thickness	BLS Mass Flow (% of passage flow)	TEB Mass Flow (% of passage flow)
Baseline (no control)	0.023	-----	0.486	-----	-----	-----
Suction Only	0.018	22%	0.381	22%	0.37	-----
Suction + Blowing 48 psig manifold press.	0.016	30%	0.351	28%	0.38	2.1
Suction + Blowing 65 psig manifold press.	0.013	43%	N/A	N/A	0.38	2.9
Suction + Blowing 70 psig manifold press.	0.012	48%	0.303	38%	0.38	3.1

Uncertainty due to instrumentation accuracy

Loss Coefficient: ±.0001

Wake Momentum Thickness: ±.012

BLS Mass Flow: ±0.01

TEB Mass Flow: ±0.1

3.3 Flow Control: Deviation-Angle Blowing

The second set of flow control experiments used the deviation-angle blowing design shown in Figure 2.5. The only blowing manifold pressure tested with the deviation-angle blowing was 70 psig, which was the highest manifold pressure attainable with the current setup and the most effective manifold pressure from the metal-angle blowing experiments. New baseline and suction-only runs were also performed for the new blade design. The new baseline and suction-only data proved to be repeatable, as shown in Figure 3.12. Figure 3.13 shows the total pressure ratio profiles of the flow control wake for the baseline, suction-only, and suction-plus-blowing tests. Figure 3.13 also includes error bars that indicate the uncertainty range of the pressure ratio profiles due to the slight variations between the repeatability runs.

Similar to the results obtained for the metal-angle design, the application of boundary layer suction delayed the onset of the wake on the suction-side of the flow control blade. However, the application of deviation-angle blowing did not result in a smaller wake than that achieved with suction alone. The wake profile for the suction-plus-blowing case was not symmetric about the wake center, and it was less symmetric than the suction-only wake. The addition of the deviation angle-blowing resulted in the losses becoming concentrated on the suction surface, but unlike the metal-angle blowing, the suction surface loss actually increased with the addition of the blowing. These blowing results, which show trends that are contradictory to previous research, were attributed to an unexpected flow field from the blowing jets.

Although the jet holes for the deviation-angle blowing design were angled to match the measured pitch location of the suction-only blade wake, the actual center of the blowing jet deviated significantly from the hole centerline. This can be seen in Figure 3.14, which shows total pressure ratio profiles of the flow control wake for suction-only, suction-plus-blowing, and a probe traverse which measured only the trailing edge blowing jets with no tunnel flow.

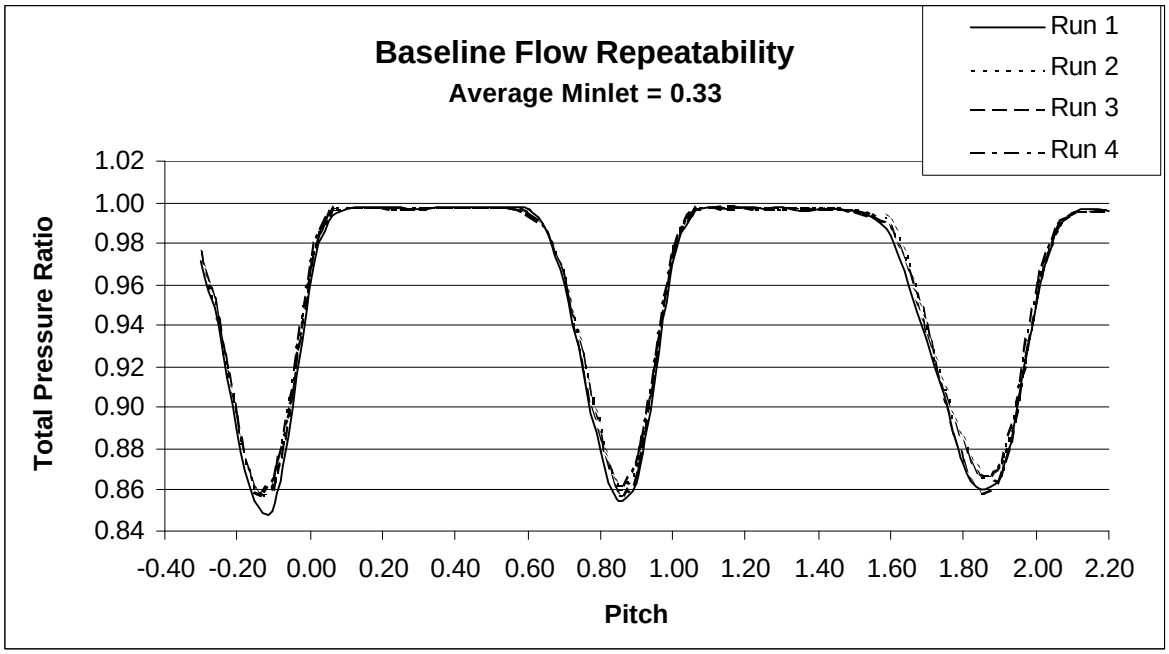

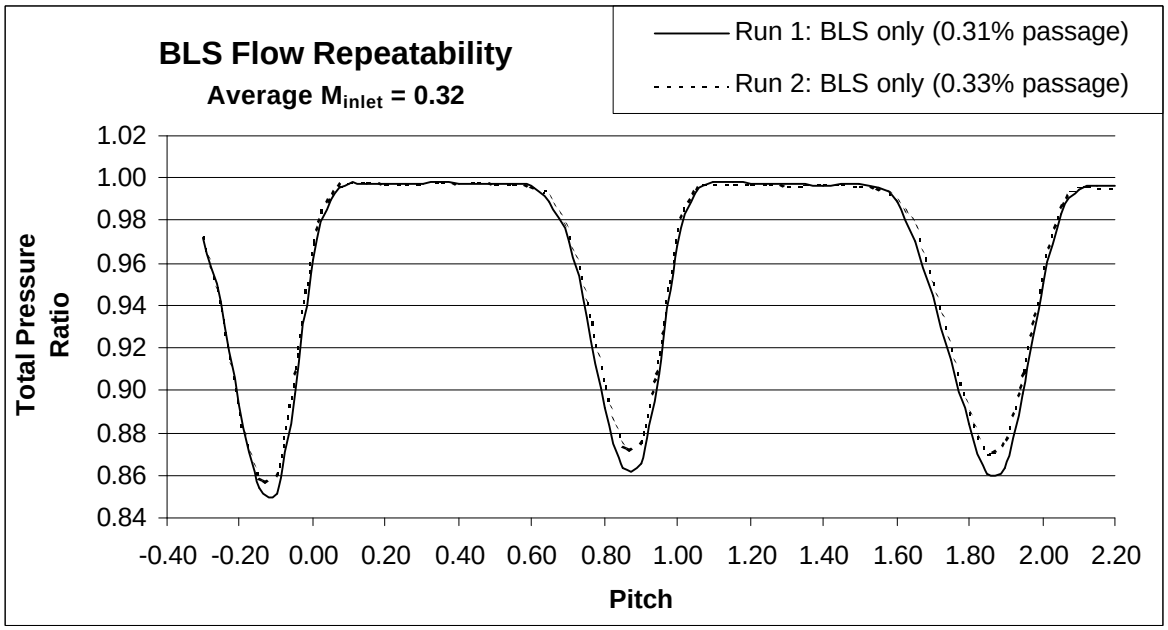

Figure 3.12 Baseline and Suction-Only Flow Repeatability, Deviation-Angle Blade

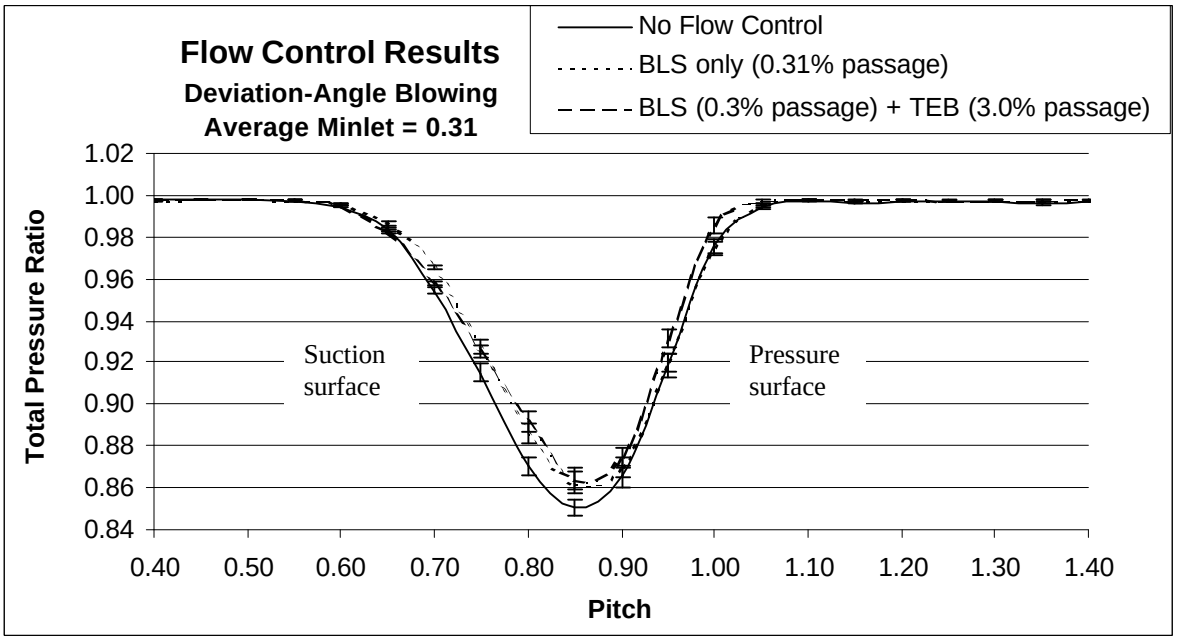

Figure 3.13 Comparison of Total Pressure Ratio Profiles for Flow Control Applied by Deviation-Angle Blade Design

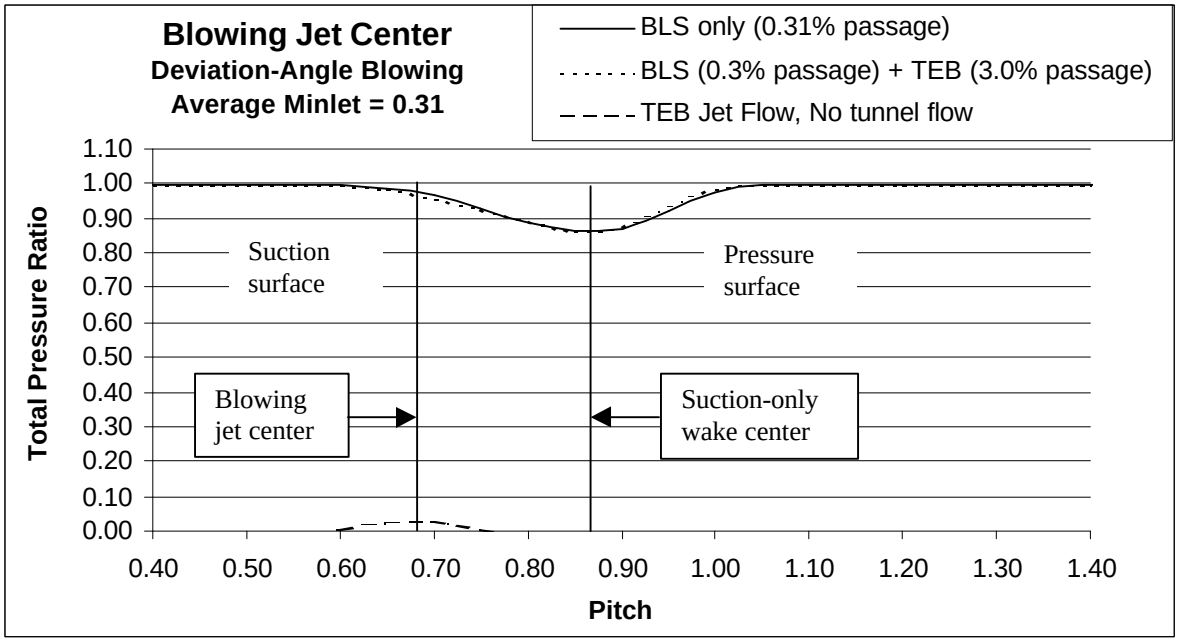

Figure 3.14 Blowing Jet Location for Deviation-Angle Blowing

While the jet hole centerline intersected the measurement plane at 0.86-pitch, the actual jet center was located at 0.68-pitch. The blowing jet deviation was attributed to a manufacturing defect and the resulting geometry of the deviation-angle blowing holes. The deviation-angle jets were machined into the same blade as the metal-angle jets. After completion of the metal-angle blowing experiments, the blowing holes through the trailing edge were filled with silver solder and ground smooth. The deviation-angle holes were then EDM machined into the blade. Due to incomplete filling of the metal-angle holes, the downstream surface of the deviation-angle holes were highly irregular. Large cavities and ridges were observed to a varying extent in all 14 of the blowing holes. Figure 3.15 shows a schematic of the actual cross-section of a typical deviation-angle blowing hole. These irregularities in the hole surface most likely caused the flow within the blowing hole to separate near the jet exit, as suggested by research related to the flow behavior of turbine film cooling holes.

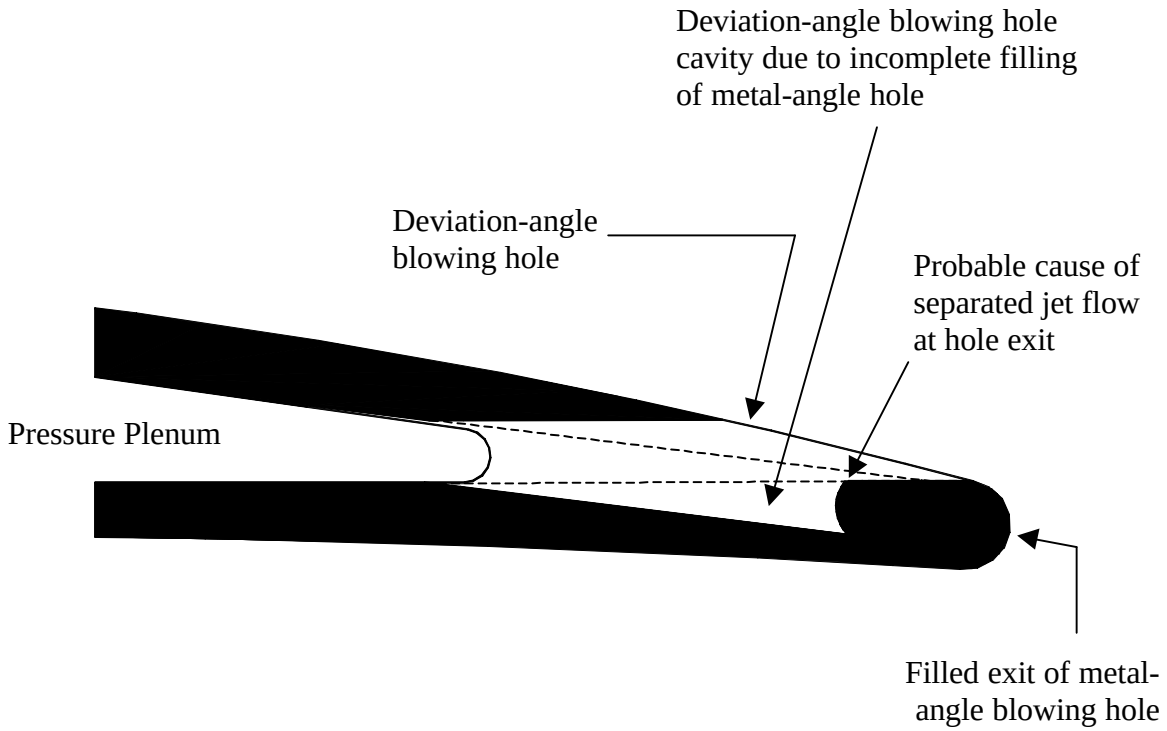

Figure 3.15 As-Machined Geometry of Deviation-Angle Blowing Holes

Pietrzyk et. al. (1989) performed an experimental study on inclined jets in a crossflow to simulate a typical film-cooled turbine blade geometry. Pietrzyk et. al.'s experiments were performed at low speeds (U_∞ = 20 m/s) on a flat plate. Laser-Doppler anemometry was used to measure the 2-D flow field behind a row of 11 jets angled 35° from the plate surface in the streamwise direction. The holes had a length to diameter ratio (L/D) of 3.5, which was purposely too short to allow for the flow exiting the jet to fully develop. Pietrzyk et. al. found that at B = 1, the velocity profile of the jet as it exited the hole was skewed upstream. The skewed profile was attributed to flow separation on the downstream side of the blowing tube initiated by a sharp corner at the tube entrance. Higher blowing ratios increased the severity of the separation and its effect on the jet velocity profile. The blowing ratio used in the deviation-angle blowing experiments was approximately 1.6. Although the deviation-angle blowing holes had a smooth entrance, the large ridges near the hole exit could trigger flow separation that created a flow field at the jet exit similar to the separated flow field near the entrance of Pietrzyk et. al.'s film cooling holes.

The deviation-angle blowing holes protruded through the suction surface of the blade rather than through the trailing edge, which resulted in a small L/D ratio of 5.8. The holes were also angled much more sharply from the blade surface in the current experiments than in Pietrzyk et. al.'s. This created large, elliptical jet openings that had a surface area more than four times greater than the area of the metal-angle jet openings. The small L/D and large exit area prevented the separated jet flow from developing the expected velocity profile at the hole exit.

The large deviation of the blowing jets from their intended exit angle and their high momentum created an aerodynamic obstruction that appears to have increased the suction surface flow separation. This is consistent with results obtained by Lee et. al. (1994), who also experimentally studied the flow characteristics of inclined jets in a cross flow. Like Pietrzyk et. al., Lee et. al.'s experiments were performed at low speeds (U_∞ = 9.65 m/s) with blowing holes angled 35° in the streamwise direction on a flat plate. Velocity ratios, R, of 0.5, 1.0, 1.5, and 2.0 were tested with a constant density ratio of 1.53. Lee et. al. found that as R increased, the injected jet penetrated the cross flow more deeply. For R = 2.0, the jet separated from the wall and maintained its structure far downstream from the injection location.

As a result of the additional separation, the addition of the deviation-angle blowing caused a slight increase in the loss coefficient and the wake momentum thickness compared to the suction-only results. This effect could be more easily seen when only the blowing was applied to the baseline flow. The application of the deviation-angle blowing to the baseline flow without suction resulted in a 14% increase of the pressure loss coefficient and a 1% increase of the wake momentum thickness. The wake center moved from 0.86-pitch for the baseline wake to 0.84-pitch for the blowing-only wake. The blowing-only wake was also less symmetric than the baseline wake. The overall increase in losses, especially on the suction surface, caused by the addition of the deviation angle blowing supported the notion that this blowing geometry generated flow separation and was detrimental to the baseline flow.

Table 3.2 summarizes the area-averaged pressure loss coefficient and wake momentum thickness results for the flow control tests performed with the deviation-angle blowing design. The average inlet Mach number was 0.31. The percent reductions presented for both the loss coefficient and the wake momentum thickness are referenced to the baseline flow obtained during that tunnel entry. The uncertainty due to instrumentation accuracy is indicated below Table 3.2 for each result. The uncertainty analysis technique used to obtain the instrumentation error bound is presented in Appendix B.

Table 3.2

Loss Coefficient and Wake Momentum Thickness Reductions Achieved with Flow Control

Deviation-Angle Trailing Edge Blowing Design

Case	Area-Avg'd. Loss Coeff.	Reduction of Loss Coeff.	Wake Momentum Thickness	Reduction of Wake Momentum Thickness	BLS Mass Flow (% of passage flow)	TEB Mass Flow (% of passage flow)
Baseline (no control)	0.035	-----	0.610	-----	-----	-----
Suction Only	0.029	17%	0.519	15%	0.33	-----
Blowing Only	0.040	14% increase	0.616	1% increase	-----	3.1
Suction + Blowing 70 psig manifold press.	0.031	11%	0.522	14%	0.33	3.0

Uncertainty due to instrumentation accuracy

Loss Coefficient: ±.0002

Wake Momentum Thickness: ±.010

BLS Mass Flow: ±0.01

TEB Mass Flow: ±0.1

Table 3.2 shows that the reductions in the loss coefficient and wake momentum thickness obtained with suction-only for the deviation-angle design were not as significant as those obtained during the tunnel entry in which the metal-angle design was tested. This was attributed to changes in the baseline flow conditions. Figure 3.16 shows baseline total pressure ratio profiles for the metal-angle and deviation-angle test entries. While the baseline flow is repeatable during each tunnel entry, the flow conditions could not be accurately reproduced from one tunnel entry to the next. The test conditions of these experiments were near the lowest capable in the Virginia Tech cascade wind tunnel, and slight perturbations in the test setup resulted in different flow conditions entering and exiting the test section. While most parameters could be carefully controlled, some parameters, such as the exact alignment of gaskets and transitions between tunnel sections, could not. For the deviation-angle blowing test, the baseline flow was more periodic, but the wakes were also deeper. This resulted in greater losses and momentum deficits for the baseline flow.

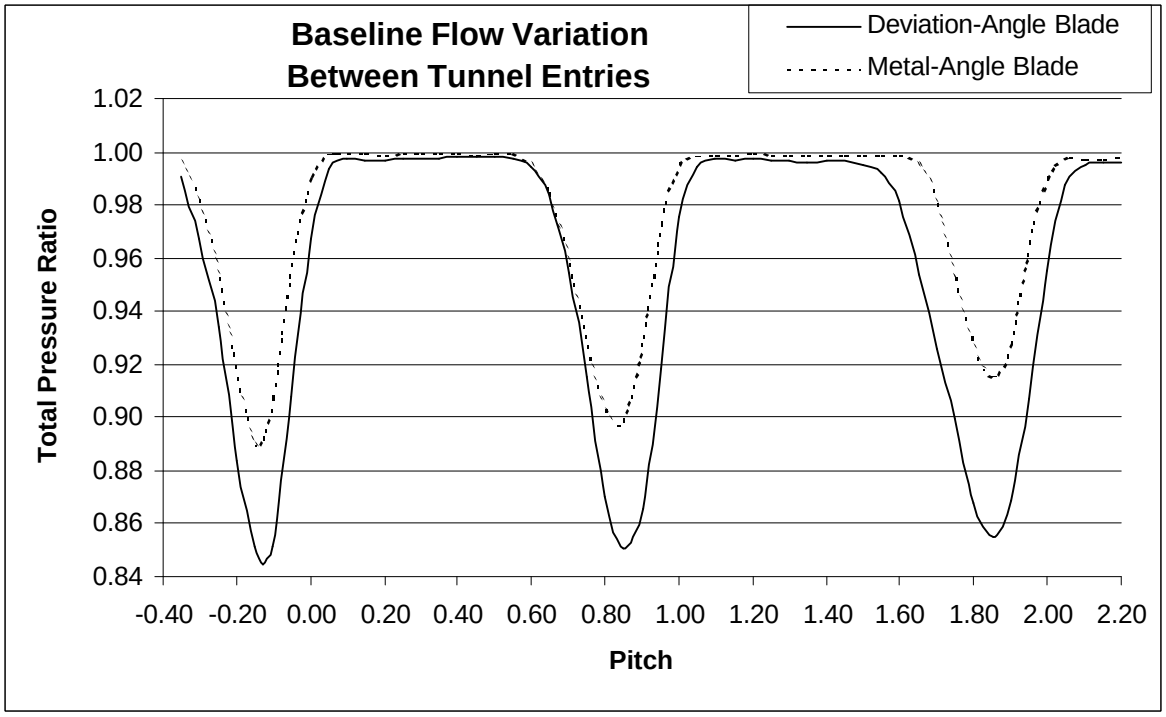

Figure 3.16 Comparison of Metal-Angle and Deviation-Angle Baseline Flows

Since the amount of mass flow added or removed by the flow control was fixed by the upper limits of the flow control equipment, the reductions achieved by suction in Table 3.2 were less than those in Table 3.1. The application of metal-angle blowing to a typical baseline wake from the deviation-angle experiments would also show smaller loss and momentum deficit reductions for the same reason.

3.4 Comparison of Current Results with Low-Speed Results in Literature

Tables 3.1 and 3.2 show that a significant reduction in the loss coefficient and the wake momentum thickness were achieved with very little flow removal by the boundary layer suction. Due to the much higher exit Mach number of the current experiments, the baseline wake of the IGV was much larger than those from previous research. The results from Table 3.1 and 3.2 show that the application of boundary layer suction was not as effective at the higher speeds because of the larger wakes. However, operation of this cascade at Mach and Reynolds numbers very similar to those of Sell's experiments (1997) yielded very similar results (see Appendix A). Regardless of the magnitude of the flow control effects, the trends of the high-speed results match well with the low-speed results from the literature.

Sell (1997) and Bons et. al. (1999) obtained experimental flow control results that were most comparable to the boundary layer suction results of this work. Both Sell and Bons et. al. performed low-speed flow control experiments on cascades of realistic blading. For both experiments, the inlet Mach number was 0.1 or less. Sell examined the use of boundary layer suction and trailing edge blowing to reduce the wake of a fan blade, and Bons et. al. examined the use of vortex generator jets (VGJ's) to reduce suction surface flow separation on a low-pressure turbine blade. The boundary layer suction results of Sell's experiments and the results of Bons et. al.'s experiments appear in Figures 3.17 and 3.18. Figures 3.19 and 3.20 show velocity profiles (u/U_∞) for the metal-angle and deviation-angle blowing experiments, respectively, for comparison.

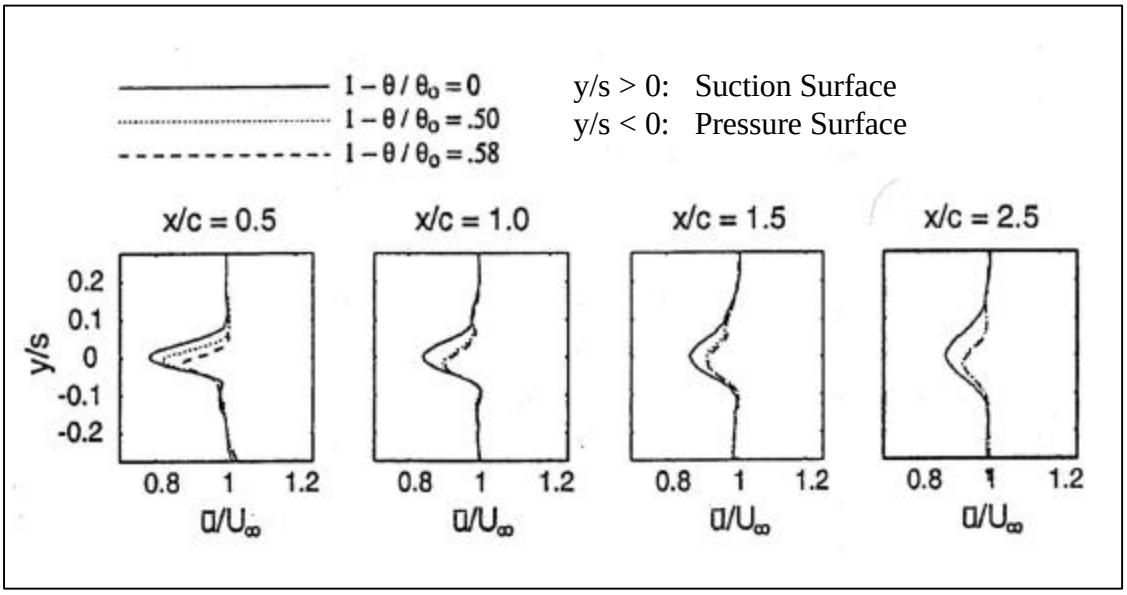

Figure 3.17 Boundary Layer Suction Results from Sell (1997). $Re_c \cong 250{,}000$, $M \cong 0.1$

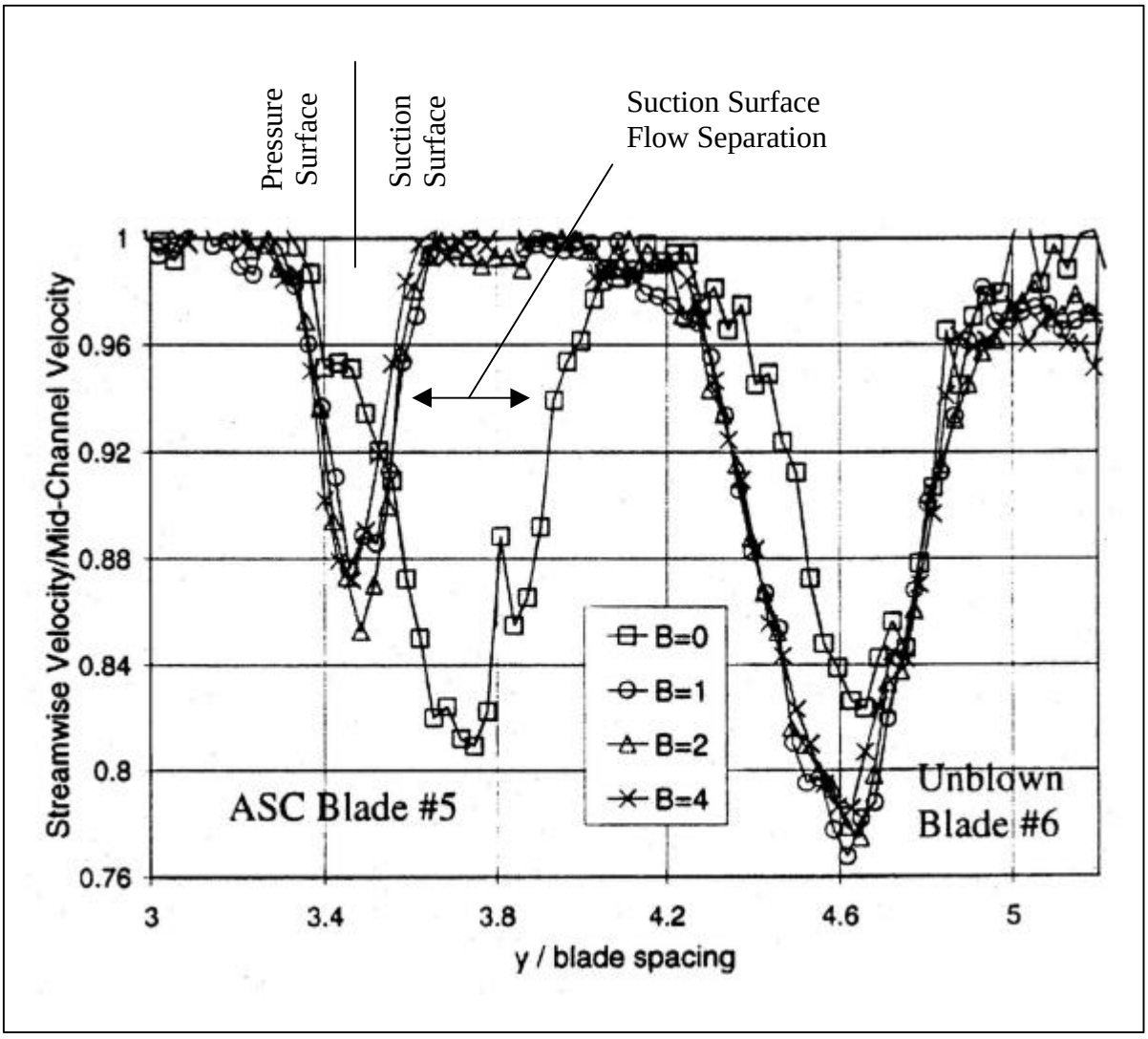

Figure 3.18 Vortex Generator Jet Results from Bons et. al. (1999). $Re_c = 50{,}000$, $M < 0.1$

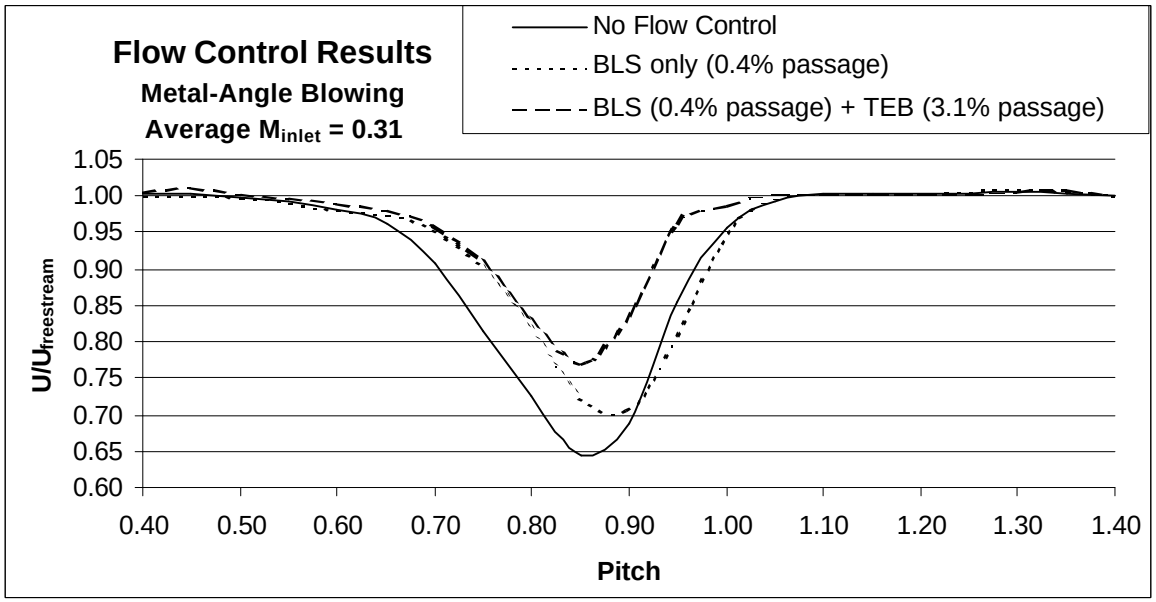

Figure 3.19 Comparison of Velocity Ratio Profiles for Flow Control Applied by Metal-Angle Blade Design

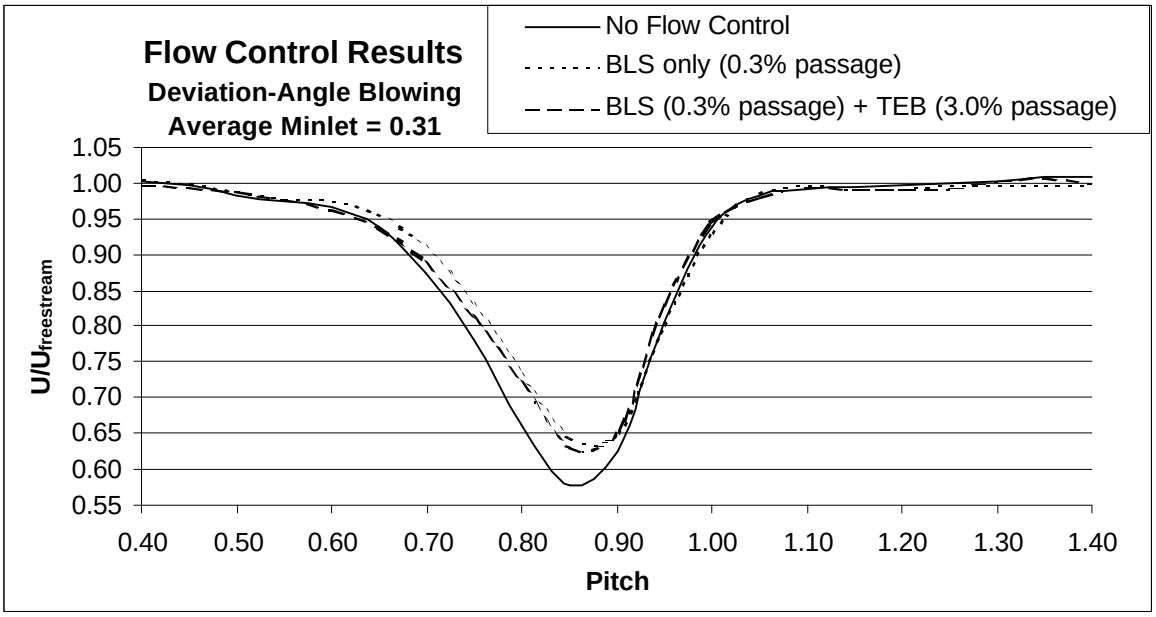

Figure 3.20 Comparison of Velocity Ratio Profiles for Flow Control Applied by Deviation-Angle Blade Design

The trends of the suction-only results of Figures 3.19 and 3.20 show good agreement with both Sell's and Bons et. al.'s results. In all cases, the application of the suction surface flow control reduced the width of the wake, and the wake peak moved in the pitch-wise direction towards the pressure surface. Sell achieved a 50% reduction in the momentum thickness by removing 1.25% passage mass flow. The momentum thickness reduction achieved by Sell was significantly greater than what was gained by the current experiments, but a much larger suction mass flow was used, and the baseline wake was much smaller in width and depth than those of the current experiment. The mass flow removal in the current experiment was limited by the capabilities of the suction system.

The mass flow removed by Sell was equivalent to 100% removal of the suction surface boundary layer at the point of suction. The baseline flow of Sell's experiment had no separation, and the suction was thus applied very near to the trailing edge (80%-chord) where the boundary layer was thickest. For subsonic separated flows, such as in this experiment, the best location for suction is near the point of separation (Kerrebrock et. al., 1998). The flow separated near the leading edge of the IGV flap at roughly x/C = 0.50. Applying suction this far upstream allowed for further development of the suction surface boundary layer downstream from the suction array (Kerrebrock et. al., 1998), which resulted in greater losses than complete removal of all viscous fluid near the trailing edge of the suction surface. For the current experiment, suction near the trailing edge was not possible due to the plenum arrangement for the trailing edge blowing. Also, per Kerrebrock et. al.'s conclusions, suction applied further downstream that equaled or bettered the current result would require much more suction mass flow.

The suction-only trends for the IGV experiments also show good agreement with the VGJ blowing results of Bons et. al. (1999). Bons et. al. achieved a 65% reduction in the wake momentum thickness of a turbine cascade operating at low speed (Re_c = 50,000) by greatly reducing suction surface flow separation. The VGJ separation control concept relies upon a different process for separation reduction than the boundary layer suction technique used in the current experiment. Boundary layer suction relies more heavily on removal of the low momentum fluid, while VGJ's rely on entrainment and mixing of the low momentum fluid with the higher momentum free stream flow. The amount of mass flow added by the VGJ's in order

to achieve the momentum thickness reduction could not be determined from the information provided in Bons et. al.

To further reduce the loss coefficient and wake momentum thickness with trailing edge blowing required a much more significant mass addition than what was used by Sell. The results of Sell's metal-angle blowing experiments appear in Figure 3.21.

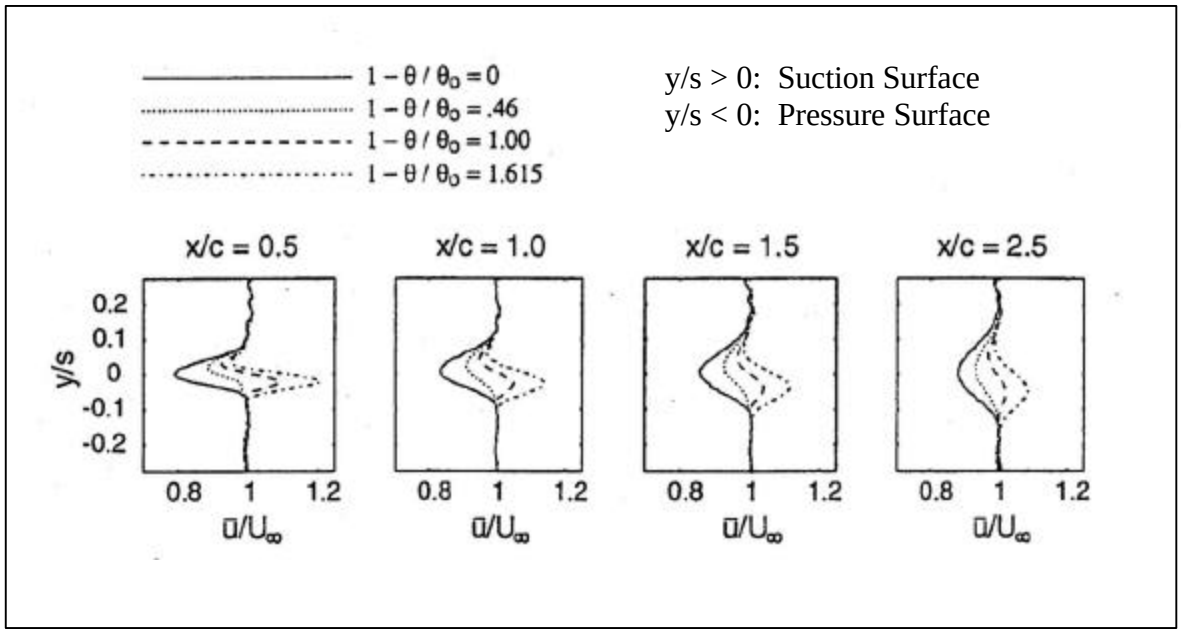

Figure 3.21 Metal-Angle Trailing Edge Blowing Results from Sell (1997)

The trends of the high-speed metal-angle blowing results from the current experiment match quite well with the metal-angle blowing results presented by Sell for the case of 54% momentum thickness reduction ($1-\theta/\theta_0 = 0.46$ in Figure 3.21). The results from the low-speed metal-angle blowing tests presented in Appendix A show nearly identical results to Figure 3.21. The deviation-angle blowing results from this experiment, however, did not correspond well with any results presented in the reviewed literature. Sell achieved 54% momentum thickness reduction with only 0.76% passage flow added, and he was able to achieve a momentumless wake with

1.02% passage flow for metal-angle blowing and with 1.08% passage flow for deviation-angle blowing. The higher blowing mass flows required for the current experiment resulted from the much higher exit Mach numbers of the IGV cascade, which generated much larger wakes. The time-averaged minimum velocity ratio for Sell's experiment was near 0.8, while the minimum velocity ratio for the IGV flow control wake was near 0.65. The IGV wakes were also significantly wider. The resulting momentum thickness for the IGV's baseline wake was 90% larger than that of Sell's fan blade wake. The much larger momentum deficits required greater mass flow inputs for effective filling.

In addition to the larger wakes, the high trailing edge blowing mass flows used in the current experiments were also a result of the non-ideal jet blowing angles. Figures 3.10 and 3.14 showed that the peaks of the blowing jets for the metal-angle and deviation-angle blowing were directed too far down-pitch and up-pitch from the wake centerline, respectively. As can be seen in these figures, a significant portion of the blowing jets' momentum was directed towards passage core flow, where there was little momentum loss. The actual trailing edge blowing mass flow required to achieve results comparable to those in Table 3.1 should be lower with the trailing edge jets directed at the measured wake center. Or, conversely, the loss and wake momentum deficit would both be reduced compared to the results of Table 3.1 with the same blowing rate and correct blowing angle.

Chapter 4.0 CONCLUSIONS AND RECOMMENDATIONS

The effectiveness of flow control on reducing the profile losses and the wake momentum deficit of a tandem IGV operating at a realistic speed was investigated. The IGV was tested in a cascade wind tunnel with a blade inlet angle of 0° and a blade exit angle of 55°. An inlet Mach number of 0.3 was used throughout the experiments, and the resulting average exit Mach number was 0.53. The Reynolds number based on the overall IGV chord length was greater than 500,000 for all tests. These flow conditions were significantly higher than those used in previous experimental turbomachinery flow control research. The flow control consisted of boundary layer suction applied in conjunction with trailing edge blowing. Two blowing designs, metal-angle blowing and deviation-angle blowing, were tested with one suction design. Results from low-speed blower tests (see Appendix A) showed that at low speeds, the current flow control design performed favorably compared to previous experimental results. Results from the high-speed baseline tests showed significant suction surface flow separation and large wakes, which generated high losses and large wake momentum deficits.

The high-speed experiments showed that the application of boundary layer suction reduced the losses and the wake momentum deficit of the flow control blade using minimal suction. Reductions in the pressure loss coefficient and wake momentum thickness of 22% were achieved using a suction mass flow of only 0.4% of the passage flow. The boundary layer suction achieved the loss and momentum thickness reductions by reducing the magnitude of the suction surface flow separation, as could be seen by comparison of the baseline and suction-only total pressure ratio profiles for the flow control wake. The trends of the results from the current experiments were similar to the suction surface flow control results presented by Sell (1997) and Bons et. al. (1999). Due to the much higher exit Mach number, the baseline wake of the IGV from the current experiment was much larger than those in Sell's and Bons et. al.'s experiments. The results from the current experiments showed that the application of boundary layer suction was not as effective at the higher speeds because of the larger wakes.

The effects of trailing edge blowing depended heavily upon the blowing geometry. Blowing holes aligned closely to the blade exit angle produced moderate results. Combined with suction,

the metal-angle blowing achieved pressure loss coefficient and wake momentum thickness reductions of 48% and 38%, respectively. The metal-angle blowing affected primarily the pressure-side of the blade wake due to flow deviation from the blade exit angle. The trends of the metal-angle blowing velocity ratio profiles were similar to those achieved in the metal-angle blowing experiments performed by Sell (1997).

Blowing holes aligned with the estimated deviation angle of the exit flow, however, proved to be detrimental to both the loss coefficient and the wake momentum thickness. This result is contradictory to the results of previous research. The trends of the deviation-angle blowing velocity ratio profiles were not consistent with any previous flow control experimental results. The contradictory results were attributed to a manufacturing defect that caused the deviation-angle blowing holes to produce a jet that was centered significantly up-pitch from the hole centerline. This, combined with a high blowing ratio of 1.6, caused further suction surface flow separation near the trailing edge of the flow control blade. The increased flow separation resulted in a slight increase of the loss coefficient and momentum thickness when compared to the suction-only case. The deviation-angle blowing experiments were therefore not truly representative of the design intent and showed the importance of the blowing hole geometry on generating a proper jet.

For both blowing designs, a blowing mass flow near 3% of the passage flow was used. This was much greater than the blowing mass flows used in previous research. The large wake momentum deficits generated by the higher exit Mach numbers of the current experiment required a high blowing mass flow for the trailing edge blowing to remain effective.

Future flow control research on this cascade should begin with deviation-angle blowing experiments using properly machined blowing holes. Correct alignment of the blowing jets will maximize the effects of the momentum input from the trailing edge blowing. It will also create a much more symmetrical wake, the importance of which was shown by Sell (1997) and Park and Cimbala (1991). The vortex generator jets (VGJ) used by Bons et. al. (1999) to control suction surface flow separation could also be investigated on this cascade. Using VGJ for separation control instead of boundary layer suction would simplify the flow control blade design. Since

VGJ flow control is a blowing technique, only one high pressure plenum would be needed to provide both separation control and wake filling. The application of periodic flow control, similar to that used by Wygnanski (1997), would also be interesting for results comparison with the current experiments. Wygnanski showed that while steady flow control became less effective at Mach numbers similar to those used in the current research, periodic flow control remained effective.

REFERENCES

Bons, J.P., Sondergaard, R., and Rivir, R.B., "Control of Low-Pressure Turbine Separation Using Vortex Generator Jets", 37th Aerospace Sciences Meeting and Exhibit, AIAA 99-0367, Reno, Nevada, January 1999.

Chen, S., "A Loss Model for the Transonic Flow Low-Pressure Steam Turbine Blades", Institute of Mechanical Engineers, C269, 1987.

Chu, L., "Effects of Mach Number and Flow Incidence on Aerodynamic Losses of Steam Turbine Blades", Masters Thesis, Mechanical Engineering Department, Virginia Polytechnic Institute & State University, Blacksburg, Virginia, March 1999.

Cimbala, J.M., and Park, W.J., "An Experimental Investigation of the Turbulent Structure in a Two-Dimensional Momentumless Wake", Journal of Fluid Mechanics, Vol. 213, pp. 479-509, 1990.

Hill, P.G., and Peterson, C.R., Mechanics and Thermodynamics of Propulsion, 2nd ed., Addison-Wesley Publishing Company, 1992.

Kerrebrock, J.L., Drela, M., Merchant, A.A., and Schuler, B.J., "A Family of Designs for Aspirated Compressors", ASME 98-GT-196, June 1998.

Lakshminarayana, B., Fluid Dynamics and Heat Transfer of Turbomachinery, John Wiley & Sons, 1996.

Lee, S.W., Lee, J.S., and Sung, T.R., "Experimental Study of the Flow Characteristics of Streamwise Inclined Jets in Crossflow on Flat Plate", Journal of Turbomachinery, Vol. 116, pp.97-105, January 1994.

Munson, B.R., Young ,D.F., and Okiishi, T.H., Fundamentals of Fluid Mechanics, 3rd ed., John Wiley & Sons, 1998.

Naumann, R.G., "Control of the Wake from a Simulated Blade by Trailing Edge Blowing", Masters Thesis, Department of Mechanical Engineering & Mechanics, Lehigh University, Bethlehem, Pennsylvania, July 1992

Park, W.J., and Cimbala, J.M., "The Effect of Jet Injection Geometry on Two-Dimensional Momentumless Wakes", Journal of Fluid Mechanics, Vol. 224, pp. 29-47, 1991.

Pietrzyk, J.R., Bogard, D.G., and Crawford, M.E., "Hydrodynamic Measurements of Jets in Crossflow for Gas Turbine Film Cooling Applications", Journal of Turbomachinery, Vol. 111, pp. 139-145, April 1989.

Poisson-Quinton, Ph., and Lepage, L., "Survey of French Research on the Control of Boundary Layer and Circulation", in Boundary Layer and Flow Control, G.V. Lachmann (Ed.), Volume 1, Pergamon Press, 1961.

Saha, U.K., and Roy, B., "On the Application of Variable Camber Blading in Axial Flow Fans and Compressors", ASME 96-TA-58, 1996.

Sell, J., "Cascade Testing to Assess the Effectiveness of Mass Addition/Removal Wake Management Strategies for Reduction of Rotor-Stator Interaction Noise", Masters Thesis, Department of Aeronautics and Astronautics, Massachusetts Institute of Technology, Cambridge, Massachusetts, February 1997.

Waitz, I.A., Brookfield, J.M., Sell, J., and Hayden, B.J., "Preliminary Assessment of Wake Management Strategies for Reduction of Turbomachinery Fan Noise", First Joint CEAS/AIAA Aeroacoustics Conference, CEAS/AIAA-95-102, Munich, Germany, June 1995.

Walls, M.W., “An Experimental Determination of the Trailing Edge Base Pressure on Blades in Transonic Turbine Cascades”, Masters Thesis, Mechanical Engineering Department, Virginia Polytechnic Institute & State University, Blacksburg, Virginia, September 1993.

Williams, J., “A Brief History of British Research on Boundary Layer Control for High Lift”, in Boundary Layer and Flow Control, G.V. Lachmann (Ed.), Volume 1, Pergamon Press, 1961.

Wygnanski, I., “Boundary Layer and Flow Control by Periodic Addition of Momentum”, 4th Shear Flow Control Conference, AIAA 97-2117, Snowmass Village, Colorado, June 1997.

APPENDIX A. PRELIMINARY DATA AND FLOW CONTROL DESIGN REFINEMENT

The flow control design process involved multiple iterations in an attempt to maximize the effects of the flow control on blade losses and wake momentum deficit. The original flow control configuration consisted of two arrays of suction holes and one array of blowing holes.

The first array of suction holes was located at the leading edge of the back tandem (at x/C = 0.48). The second array of suction holes was the same one described in Section 2.2.2. The holes of the first suction array were also 1/32-inch in diameter with 0.08 inch center-to-center spacing. They were angled towards the incoming flow at 64° from the local blade surface.

The original trailing edge blowing design placed one array of 26 blowing holes located at the trailing edge of the back tandem (x/C = 1). The hole array consisted of 1/32-inch diameter holes equally spaced 0.08 inches from center to center. The blowing holes were angled approximately 1.5° up-pitch from the blade exit angle and spanned the center two inches of the blade. This deviation angle was the maximum angle that could be machined into the trailing edge of the blade without requiring the holes to protrude through the blade's suction surface. Figure A.1 shows a cross-section of the original flow control blade design.

Several baseline experiments in front of a low speed blower and in the wind tunnel were used to evaluate the potential of both the original design described above and iterations of this design before presenting the data discussed in the body of this paper. The blower experiments, discussed in Section A.1, were useful in refining the boundary layer suction configuration. The preliminary tunnel experiments, described in Section A.2, were useful in refining the trailing edge blowing configuration.

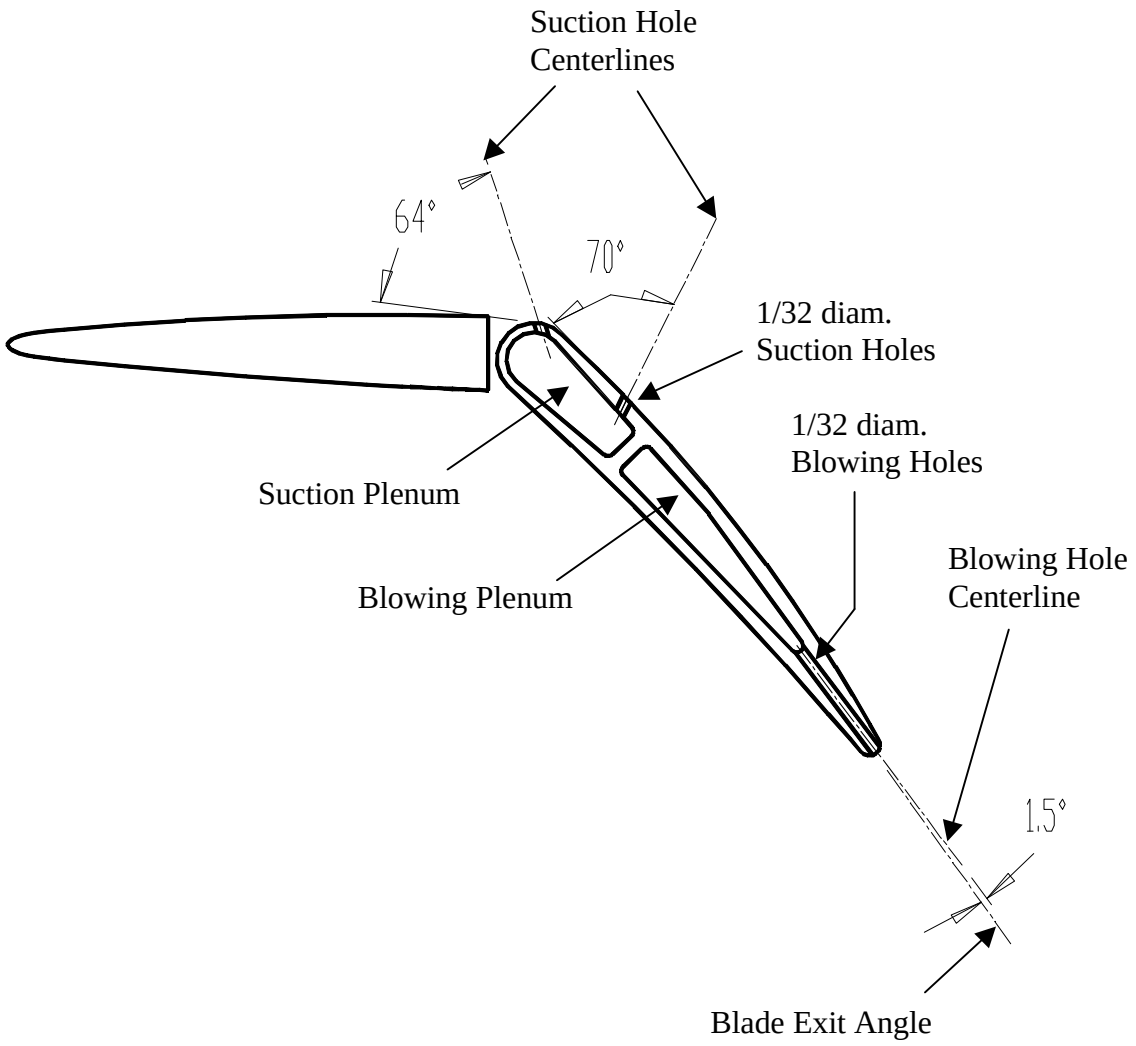

Figure A.1 Cross-Section of Original Flow Control Blade Design

A.1 Low-Speed Blower Test

Several low-speed tests were performed in front of a centrifugal blower to gain experience adjusting the ejector pump and also to test the flow control design. The following sections briefly explain the setup and results of the blower tests.

A.1.1 Blower test setup

For the blower tests, the blade cascade was fully assembled with the 40° flap angle as it would be installed in the wind tunnel. The cascade was installed in a wooden test section mounted on an adjustable tripod oriented such that the IGV's directed the flow upwards. The cascade was placed in front of a centrifugal blower with a four-inch by four-inch square nozzle. This blower/nozzle configuration provided a sustained cascade inlet velocity of 45 m/s. The flow control blade was centered in front of the nozzle, resulting in full flow through the passages above and below the flow control blade over the center four inches of its span.

Another tripod with a manually-adjustable traverse was placed to the side of the cascade. A Pitot-static probe was installed in the traverse, and its location was adjusted so that it measured along the same streamwise plane as the traverse probe would in the wind tunnel. The tip of the probe was angled to match the exit angle of the IGV's. The total pressure and static pressure outputs of the Pitot-static probe were connected to separate 0 to 3 psid MKS differential pressure transducers. The reference pressure connection of each transducer was exposed to the atmosphere so that the transducers would display pressures in psig. The probe was manually traversed across the wake of the flow control blade, and at set intervals, the downstream static pressure and downstream total pressure were manually recorded. The upstream total and static pressures were also measured with the Pitot-static probe. Figure A.2 shows a schematic of the blower test setup.

The boundary layer suction equipment used in the blower experiment was identical to that used in the wind tunnel, as described in Section 2.4. The trailing edge blowing equipment was identical except for the orifice plate assembly. At the time of this experiment, no suitable devices were available for measuring the trailing edge blowing mass flow. A 2000 psig compressed air tank supplied the high pressure air required to run the ejector pump, and a 70 psig shop air line supplied the high pressure air required for the trailing edge blowing.

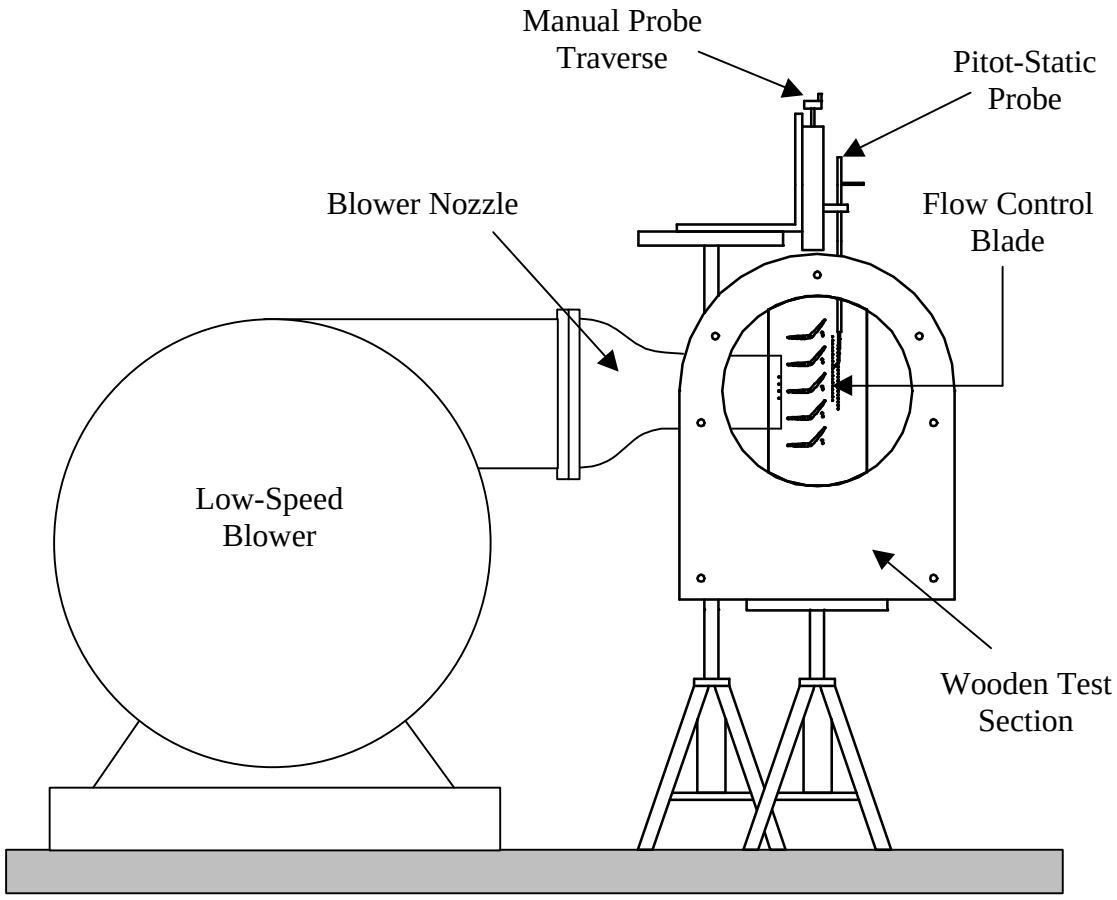

Figure A.2 Low Speed Blower Test Setup

A.1.2 Blower test results

Typical results from the blower experiments appear graphically as velocity ratio profiles in Figure A.3 and numerically in Table A.1. Figure A.3 shows severe flow separation that, pitch-wise, affected nearly half of the flow control passage. The suction side separation was greatly reduced with just the boundary layer suction. However, still assuming a C_Q of 0.009 for flow reattachment, the measured suction mass flow was more than three times greater than the predicted minimum suction mass flow for the blower inlet conditions. The measured suction mass flow was also about 40% greater than the predicted required suction mass flow when operating at the wind tunnel conditions. Poisson-Quinton and Lepage (1961) and Sell (1997) indicated that additional suction mass flow beyond that which is required to reattach the separated flow or completely remove the blade boundary layer provides negligible benefit.

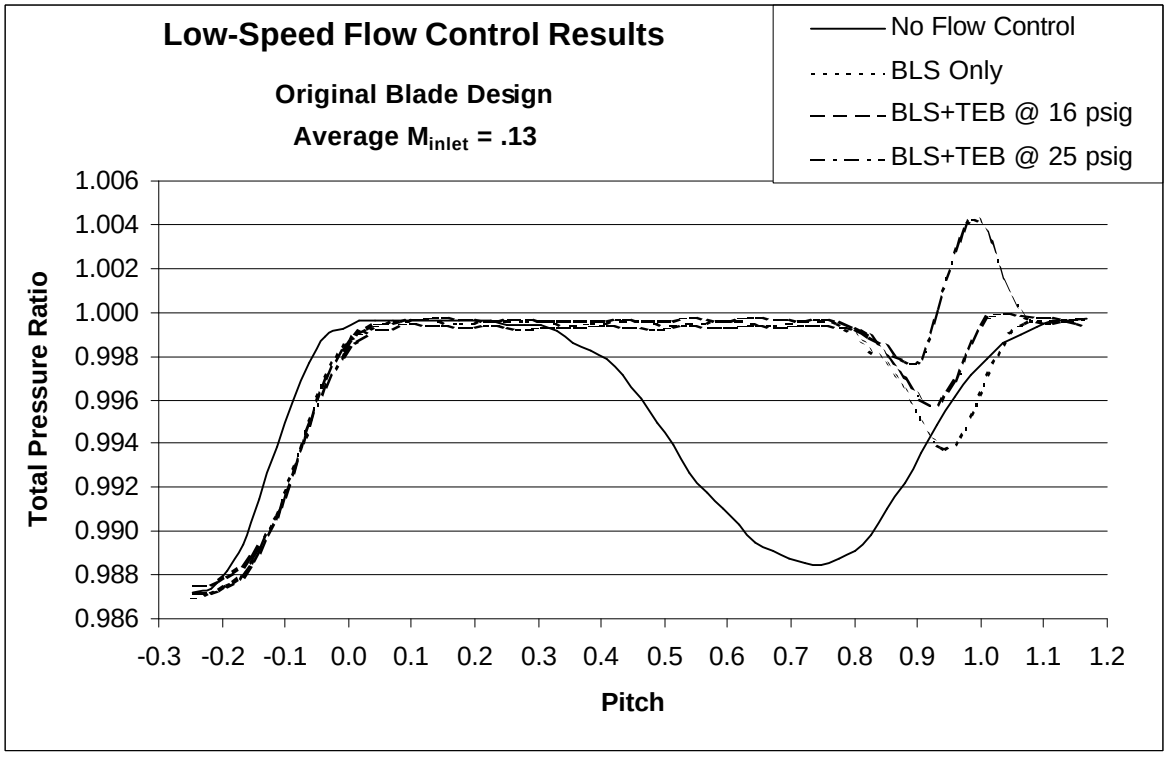

Figure A.3 Comparison of Total Pressure Ratio Profiles from Low Speed Flow Control Tests

Table A.1

Loss Coefficient and Wake Momentum Thickness Reductions Achieved during Low-Speed Flow Control Tests

Case	Area-Avg'd. Loss Coeff.	Reduction of Loss Coeff.	Wake Momentum Thickness	Reduction of Wake Momentum Thickness	BLS Mass Flow (% of passage mass flow)
Baseline (no control)	0.0095	-----	1.006	-----	-----
Suction Only	0.0024	75%	0.193	81%	2.4
Suction + Blowing 16 psig manifold press.	0.0014	84%	0.088	91%	2.4
Suction + Blowing 25 psig manifold press.	.0006	94%	-0.120	112%	2.4

The Reynolds number based on the overall IGV chord length was approximately 230,000 for the blower test. At Reynolds numbers in the 200,000 to 250,000 range, the tendency for boundary layers to be laminar and their tendency to separate increase (Lakshminarayana, 1996). At the higher speed of the wind tunnel tests, the Reynolds number was more than 500,000, and the flow separation to be corrected by suction was less severe than that seen in the blower tests. Based on the C_Q estimate and the Reynolds number argument, it was decided that the available boundary layer suction mass flow of the original design was excessive. In order to minimize the amount of air removed from the IGV passage, the front row of suction holes were temporarily sealed with epoxy. It was assumed that the back array of suction holes, which were located closer to the beginning the separated region seen in the Schlieren photographs, would more effectively reduce the separation.

Due to the low flow velocity exiting the IGV passage, the suction-only wake had a small momentum deficit, and hence the trailing edge blowing required very low mass flows for effective wake filling. Even at relatively low plenum pressures, a spike in the velocity ratio profile appeared (as can be seen in Figure A.3). This resulted in the negative momentum thickness presented in Table A.1, indicating that too much momentum was introduced into the flow by the blowing jets.

The results and trends from Table A.1 and Figure A.3 match very well with Sell's results (See Figures 3.17 and 3.21). This was expected since the low-speed blower test operated at flow conditions similar to Sell's cascade tests ($Re \cong 230{,}000$ and $M_1 \cong 0.1$ for the blower test, $Re \geq 250{,}000$ and $M_1 \cong 0.1$ for Sell's tests). Due to the large separation observed for this blade at these inlet conditions, the low-speed boundary layer suction results for the current cascade were significantly greater than the results presented by Sell (1997), although a much higher suction flow rate was used. At the low speeds of the blower test, it was also quite easy to generate momentumless and negative-deficit wakes nearly identical in shape to the metal-angle blowing wakes achieved by Sell.

A.2 Preliminary Tunnel Tests – Original Trailing Edge Blowing Design

Several sets of preliminary wind tunnel tests were performed to experimentally determine the Mach number capabilities (inlet and exit) of the IGV cascade and to test the functioning of the probe traverse, data acquisition, and the flow control systems. The following sections briefly explain the setup and results of the preliminary tunnel tests and their influence on the trailing edge blowing design.

A.2.1 Preliminary wind tunnel test setup

The experimental setup used for the preliminary tunnel tests was identical to the setup described in Chapter 2 except for the data acquisition system. In these preliminary tests, a data acquisition system consisting of an eight-channel LeCroy 8013A high-speed data acquisition unit controlled by a personal computer was used in place of the Labview system. The LeCroy was capable of acquiring up to eight channels and was set with a sampling rate of 50 Hz. The LeCroy recorded the upstream total pressure, upstream total temperature, differential total pressure, and traverse position. The differential pressure transducer used in these experiments had a 0 to 20 psid pressure range over a 0 to 10 VDC full-scale output voltage, as opposed to the 0 to 3 psid transducer used in the Chapter 2 setup.

The boundary layer suction and trailing edge blowing setups used in the preliminary experiments were identical to those described in Section 2.4. The flow control blade design consisted of the one array of suction holes at x/C = 0.59 and the blowing configuration described at the beginning of Appendix A.

A.2.2 Preliminary wind tunnel test results

Typical results from the preliminary tunnel experiments appear in Figure A.4. This figure compares the total pressure ratio profiles from a baseline, suction-only, and a suction-plus-blowing case to judge the effectiveness of the original trailing edge blowing design. The most dramatic result shown in this figure is the unacceptable level of signal noise in the data

acquisition system. No loss coefficients or wake momentum thicknesses were calculated due to the signal noise. Graphically, it appears from Figure A.4 that the trailing edge blowing provided some wake filling, but the reductions in the pressure loss and the wake momentum deficit that were achieved were not significant. The blowing mass flow used to achieve these results was approximately 0.7% of the passage flow. The uncertainty of the orifice meter at this mass flow, however, was near 15%. The blowing plenum pressure used to obtain these results was the maximum that the blowing supply system would allow. To further increase the blowing mass flow and the injected momentum required more exit area. This was achieved by boring fourteen adjacent blowing holes centered on the blade span to a larger diameter. The six remaining holes at each end of the blowing span were sealed so that there would be little net change in the amount of mass flow required to supply the blowing plenum. These modifications resulted in the metal-angle blowing design presented in Chapter 2.

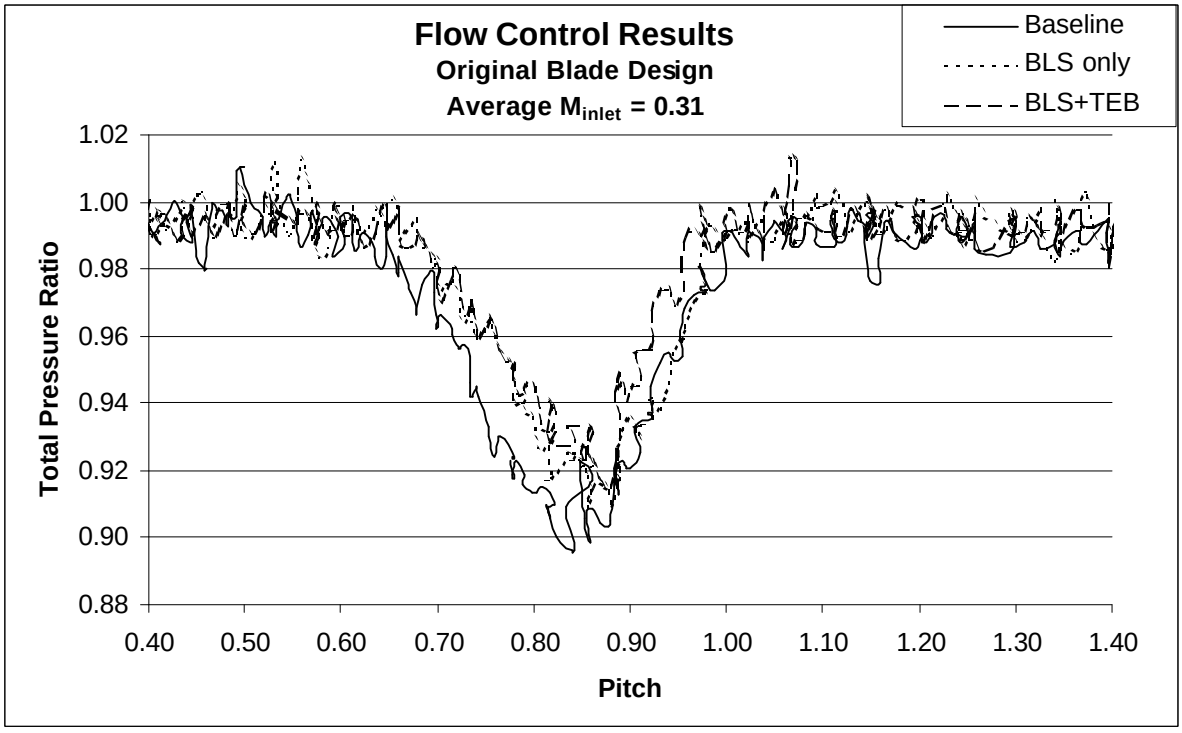

Figure A.4 Comparison of Total Pressure Ratio Profiles from Wind Tunnel Tests of Original Flow Control Blade

The signal noise that rendered the acquired data unacceptable for calculation purposes was also the motivation behind implementing the new data acquisition system for further tunnel experiments. Previous attempts to filter the signals acquired by the LeCroy with RC filters had been unsuccessful do to unexplained signal clipping unrelated to the filter's cutoff frequency. The Labview data acquisition system had proven to be more user friendly, more stable, and produced much cleaner signals in later experiments.

APPENDIX B UNCERTAINTY ANALYSIS

The experimental uncertainties for the cascade tests fall into two categories: uncertainty due to instrumentation accuracy, and uncertainty due to slight variance in flow conditions from one run to the next. Errors due to instrumentation accuracy are reflected in the measured parameters (P_t, P, T_t, DP, etc.). Table B.1 lists each of the measurement instruments used in these experiments and their associated uncertainties, as determined from manufacturer's catalogs or from prior experimental investigations (see Walls, 1993).

Table B.1

Instrumentation Uncertainties

Instrument	Measurement	Instrument Uncertainty
MKS pressure transducer, 0-3 psid	DP	±0.0015 psi
Validyne pressure transducer, 0-8.9 in. H_2O	Laminar Flow Element DP	±0.022 in. H_2O
Validyne pressure transducer, 0-20 psig	Laminar Flow Element upstream P	±0.05 psi
Validyne pressure transducer, 0-3.2 psid	Orifice meter DP	±0.008 psi
Type K Thermocouple	T_{t1}	±2 K
P_{t1} pressure tranducer 0-100 psig	P_{t1}	±0.036 psi
PSI pressure scanner ± 15 psig	P_1, P_2	±0.03 psi
Laminar Flow Element 0-100 cfm	Boundary Layer Suction volumetric flowrate	±0.004 cfm

The instrumentation uncertainties presented in Table B.1 propagate and compound as the measured quantities are manipulated to determine the calculated results. The two major results presented from this experiment were the total pressure loss coefficient and the wake momentum thickness. The loss coefficient was determined from Equation 2.7.1. The uncertainty of this calculation due to the instrumentation accuracy was determined from Equation 2.7.1 and Equation B.1:

$$dw = \sqrt{\left[\left(\frac{\partial w}{\partial P_{t1}}\right)dP_{t1}\right]^2 + \left[\left(\frac{\partial w}{\partial DP}\right)dDP\right]^2} \tag{B.1}$$

The momentum thickness was determined from Equation 2.7.3. The uncertainty of this calculation due to the instrumentation accuracy was determined from Equations 2.7.3, 2.7.5, 2.7.6, and Equations B.2 through B.4:

$$d(q/d) = \sqrt{\left[\left(\frac{\partial(q/d)}{\partial u}\right)du\right]^2 + \left[\left(\frac{\partial(q/d)}{\partial U_\infty}\right)dU_\infty\right]^2} \tag{B.2}$$

$$du = dU_\infty = \sqrt{\left[\left(\frac{\partial u}{\partial M}\right)dM\right]^2 + \left[\left(\frac{\partial u}{\partial T}\right)dT\right]^2} \tag{B.3}$$

$$dM = \sqrt{\left[\left(\frac{\partial M}{\partial P_t}\right)dP_t\right]^2 + \left[\left(\frac{\partial M}{\partial P}\right)dP\right]^2 + \left[\left(\frac{\partial M}{\partial DP}\right)dDP\right]^2} \tag{B.4}$$

Similar expressions for the uncertainty of the suction mass flow, blowing mass flow, and total pressure ratio were also derived. The uncertainties due to instrumentation accuracy for each of the calculated quantities presented in Chapter 3 appear in Table B.2.

Table B.2

Uncertainty due to Instrumentation Accuracy

Calculated Quantity	Uncertainty Range
ω	±0.42% minimum to ±0.93% maximum
θ/d	±1.5% minimum to ±4.0% maximum
M	±0.75% minimum to ±0.94% maximum
Passage mass flow	±2.3% minimum to ±2.6% maximum
Suction mass flow	Less than ±0.1%
Blowing mass flow	±1.7%
Total pressure ratio	Less than ±0.1%

Some uncertainty was also introduced by slight variations in the tunnel conditions experienced from one tunnel run to the next. The tunnel flow variance was a function primarily of the control system's ability to accurately reproduce the tunnel inlet conditions. These slight variations are apparent in all of the repeatability plots presented in Chapter 3. The flow variance uncertainty was displayed with error bars in Figures 3.7 and 3.13. The total pressure ratio profiles and error bar ranges in these figures were derived from the averages and standard deviations of the measured pressure ratio profiles for each of the repeatability cases.

VITA

Thomas W. Vandeputte

Thomas Vandeputte was born in New Brunswick, New Jersey on June 7, 1974. He graduated *Summa Cum Laude* from Bucknell University in Lewisburg, PA with a Bachelor of Science in Mechanical Engineering in 1996. After working for two years as a mechanical engineer at Corning Incorporated, he began graduate studies at Virginia Tech under the guidance of Dr. Wing F. Ng. In addition to his research, the author also competed for the Virginia Tech men's gymnastics team. The author defended his work on January 19, 2000. Upon graduation, the author began work at GE Gas Turbines in Greenville, SC.